Multiproxy reconstruction of late quaternary upper ocean temperature in the subtropical southwestern Atlantic

Joana Cruz, Ioanna Bouloubassi, Arnaud Huguet, Alice M.S. Rodrigues, Thiago Santos, Igor Venancio, Douglas Lessa, Rodrigo Sobrinho, Rodrigo Nascimento, Marcelo Bernardes

Multiproxy reconstruction of late Quaternary upper ocean temperature in the Subtropical Southwestern Atlantic

Joana F. Cruz*[1], Ioanna Bouloubassi[2], Arnaud Huguet[3], Alice M. S. Rodrigues[1], Thiago P. Santos[1], Igor M. Venancio[1], Douglas Lessa[1], Rodrigo L. Sobrinho[1], Rodrigo A. Nascimento[1], Marcelo C. Bernardes[1]

[1]Department of Geochemistry, Federal Fluminense University, Niterói, Brazil.

[2]Laboratoire d'Océanographie et du Climat: Expérimentations et approches numériques (LOCEAN/IPSL), Sorbonne Université, Campus Pierre et Marie Curie, Paris, France.

[3]Sorbonne Université, CNRS, EPHE, PSL, UMR METIS, Paris, France.

*Corresponding author: Joana F. Cruz (joanafcruz@gmail.com)

ABSTRACT

Paleoceanographic studies addressing the oceanographic variability in the western sector of the subtropical South Atlantic - especially those focused on the Brazil Current (BC) and on a time scale that reaches marine isotope stage (MIS) 5 - are still rare when compared with equivalent studies carried out in the Northern Hemisphere. In order to close the data gap prior to the last 75 ka, in an unprecedented approach in this region, we reconstructed the upper temperature variations in the Subtropical Southwestern Atlantic (SSWA) between late MIS 6 and the onset of MIS 4 from organic proxies, using a marine sediment core (GL-1090). Sea temperature records derived from alkenone-based $U^{K'}_{37}$ and isoprenoid glycerol dialkyl glycerol tetraethers (isoGDGTs)-based TEX^{H}_{86} proxies were compared with those previously obtained from the same core via *Globigerinoides*

ruber (*G. ruber*) Mg/Ca and planktonic foraminifera Modern Analog Technique (MAT). The temporal variations of the temperature estimates derived from the $U^{K'}_{37}$ and TEX^{H}_{86} indexes showed similar patterns, even though the absolute $U^{K'}_{37}$ temperatures were systematically lower than those derived from TEX^{H}_{86}. Such a difference was related to the different habitat depths of alkenones and isoGDGTs source organisms of – haptophyte algae and marine *Thaumarchaeota*, respectively. The temperature estimates from TEX^{H}_{86} match the range of Mg/Ca and MAT-derived temperatures between 0 and 10 m depth, suggesting that these proxies reflect mixed layer temperatures. In contrast, the temperature estimates derived from $U^{K'}_{37}$ were close to the MAT values at between 0 and 100 m and to those derived from TEX^{H}_{86} between 0 and 200 m depth, demonstrating that the $U^{K'}_{37}$ proxy recorded temperatures from the upper thermocline. During MIS 5e, the difference in temperature estimates from TEX^{H}_{86} and $U^{K'}_{37}$ was reduced due to more prominent warming, probably related to a change in the thermal structure of the photic zone. Comparison of our data with studies of intensity and salinity anomalies of the Agulhas Current indicates a connection between the intensification of the Agulhas Leakage and the heat storage in the upper thermocline in the SSWA during MIS 5e. Our data suggest that the joint use of TEX^{H}_{86} and $U^{K'}_{37}$ is a promising approach to estimating paleoceanographic changes in the upper thermocline.

KEYWORDS: Alkenones; GDGTs; Subtropical Southwestern Atlantic; Last Interglacial

1. INTRODUCTION

Paleoclimate studies based on geochemical data contribute to climate modeling by providing a record of past natural climate oscillations beyond instrumental periods (Hansen et al., 2016; Otto-Bliesner et al., 2016). In this context, studies focusing on the

reconstitution of past climate variability help to understand changes that occurred in a climate similar to the present. The Marine Isotope Stage (MIS) 5e (129 - 116 thousand of years BP, hereafter – "ka"), also known as the Last Interglacial (LIG), has been widely studied in climate change investigation because it is the most recent period in which the planet was warmer than it is in the present-day and due to its similarity to the pre-industrial atmospheric greenhouse gas levels and high sea level (Turney and Jones, 2010; Capron et al., 2014; Govin et al., 2015; Otto-Bliesner et al., 2016; PAGES, 2016).

Paleoceanographic studies addressing the oceanographic variability in the western sector of the subtropical South Atlantic - especially those focused on the Brazil Current (BC) and on a time scale that reaches MIS 5 - are still rare when compared with equivalent studies conducted in the Northern Hemisphere. Most of the sea surface temperature (SST) reconstructions from the BC focus on the last 75 ka (Lourenço et al., 2016; Pereira et al., 2018; Dauner et al., 2019; Luz et al., 2020) and/or the Holocene (Pivel et al., 2013; Chiessi et al., 2014; Cordeiro et al., 2014; Evangelista et al., 2014; Lessa et al., 2014; Wainer et al., 2014; Chiessi et al., 2015; Lessa et al., 2016; Luz et al., 2020). The few temperature reconstructions for the BC that include MIS 5 were obtained from single proxies, such as planktonic foraminifera transfer function and Mg/Ca ratio (Portilho-Ramos et al., 2015; Lessa et al., 2017; Santos et al., 2017a; Santos et al., 2017b).

Since the reconstruction of sea paleotemperatures is based on proxies derived from marine organisms, SST estimates may be affected by the ecological preferences of these organisms. The most common organic geochemical proxies used to reconstruct SSTs are (i) alkenones synthesized by haptophyta algae (Brassell et al., 1986), through the $U^{K'}_{37}$ index (Prahl and Wakeham, 1987), and (ii) isoprenoid glycerol dialkyl glycerol tetraethers (isoGDGTs) from marine *Thaumarchaeota*, through the TEX_{86} index (Schouten et al., 2002). A multiproxy SST approach can help to assess the individual

proxy responses and can provide more confidence in the interpretations of how climate signals are being recorded (Mann et al., 1998; Leduc et al., 2010). Moreover, applying a multiproxy reconstruction in the same sediment core will reflect conditions from the same time period without chronological uncertainties (Huguet et al., 2011; Ausín et al., 2019).

This study is the first reconstruction of temperature variations at the upper ocean in the Subtropical Southwestern Atlantic (SSWA) using organic proxies from late -MIS 6 to the onset of MIS 4. Here, we investigated possible discrepancies in temperatures reconstructed by organic proxies, what factors may have caused such differences and we evaluated the responses of these proxies to the regional dynamics during the LIG. Sea temperatures were reconstructed from the same sediment record using the $U^{K'}_{37}$ and TEX_{86} indexes, respectively derived from alkenones and isoGDGTs. The corresponding results were compared with studies of intensity and salinity anomalies of the Agulhas Current.

2. STUDY AREA

The Santos Basin is located on the southeastern Brazilian continental margin, limited to the north by the Campos Basin and to the south by the Pelotas Basin. The upper ocean circulation (0 - 600 m) in this region is controlled by the BC, which originates from the southern branch of the South Equatorial Current (SEC) (10 – 14 °S) (Peterson and Stramma, 1991) and flows southward along the Brazilian margin (Stramma and England, 1999) (Fig. 1a). The upper layer of the BC (0 – 100 m depth) carries Tropical Water (TW) − a warm (> 20 °C), saline (> 36) and oligotrophic water mass influenced by high solar radiation, the wind field and excessive evaporation (Peterson and Stramma, 1991; Campos et al., 1995; Stramma and England, 1999; Silveira et al., 2000). The South Atlantic Central Water (SACW) corresponds to the bottom layer of the BC (100 – 600m depth; Fig. 1c) and is colder (~ 6 – 20 °C), less saline (34.6 – 36) and richer in nutrients

than the TW. The SACW flows in the thermocline layer and is formed in two sites: (i) in the Brazil-Malvinas Confluence (BMC) region, where the BC encounters the northward-flowing Malvinas Current (MC) (Peterson and Stramma, 1991) (Fig. 1a) and (ii) in the eastern region, via the Agulhas Leakage, bringing Indian Ocean Central Water into the South Atlantic (Richardson, 2007). The water masses that compose the deepest layers of the region are the Antarctic Intermediate Water (AAIW) (600 – 1200 m depth, northward direction), the Upper Circumpolar Deep Water (UCDW) (1200 – 1500 m depth, northward direction) and the North Atlantic Deep Water (NADW) (1500 – 2000 m depth, southward direction) (Stramma and England, 1999; Campos et al., 1995; Campos et al., 2000; Piola et al., 2000; Piola and Matano, 2001; Schmid, 2014; Silveira et al., 2000; Fig. 1c).

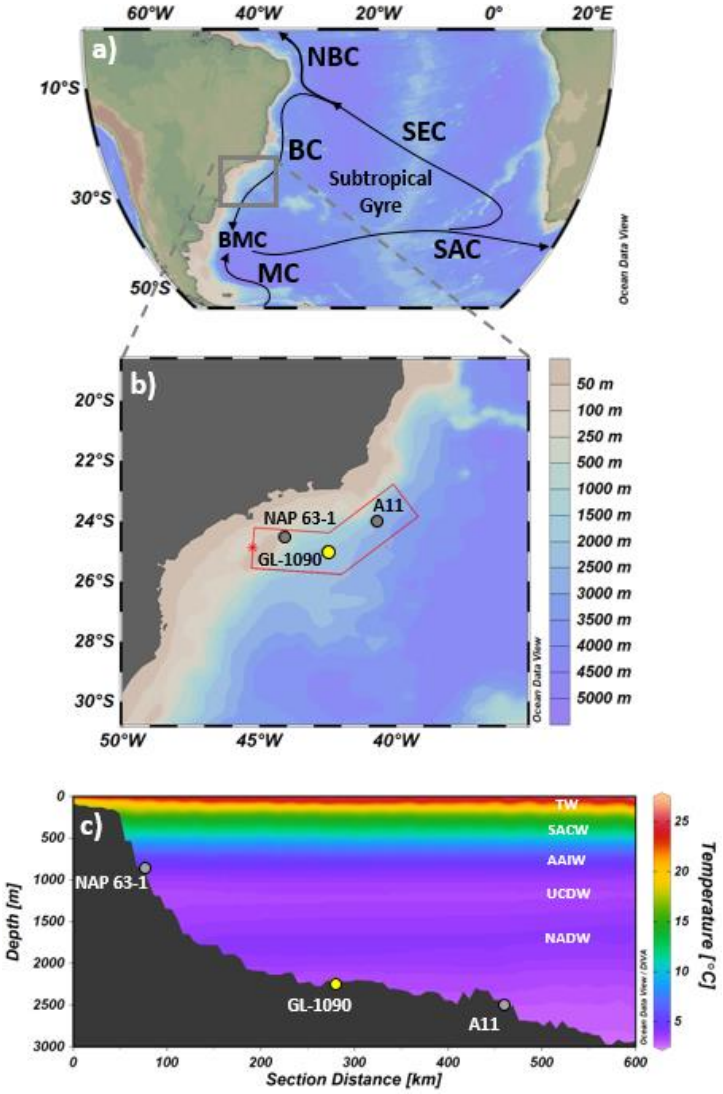

113

114 Fig. 1: Oceanographic setting of the study area and location of sediment core GL-1090.
115 (a) South Atlantic surface circulation with the main currents of the South Atlantic
116 subtropical gyre: (BC) Brazil Current; (BMC) Brazil-Malvinas Confluence; (MC)
117 Malvinas (Falkland) Current; (NBC) North Brazil Current; (SAC) South Atlantic Current;
118 and (SEC) South Equatorial Current (modified from Stramma and England, 1999). (b)
119 Zoom of the study area (gray rectangle in a) with the position of core GL-1090 (this study)
120 and cores used in the discussion: downcore NAP63-1 (Dauner et al., 2019) and core-top
121 A11 (Ceccopieri et al., 2018). (c) Vertical section of the first 3000 m water depth of the
122 Santos Basin (highlighted red section in b) showing the cores mentioned above and the
123 water masses that compose the region: (TW) Tropical Water, (SACW) South Atlantic

Central Water, (AAIW) Antarctic Intermediate Water; (UCDW) Upper Circumpolar Deep Water and (NADW) North Atlantic Deep Water. This figure was partly created with the software Ocean Data View (Schlitzer, 2003). (For interpretation of the references to color in this figure legend, the reader is referred to the web version of this article.)

Instrumental data show that the annual mean SST of the TW (0 m depth) is 24 °C, with the lowest SST (22.2 °C) during austral winter and the highest SST (25.8 °C) during austral summer (Locarnini et al., 2013). The difference in temperature between summer and winter is most pronounced in the upper 20 m of the water column (Fig. 2).

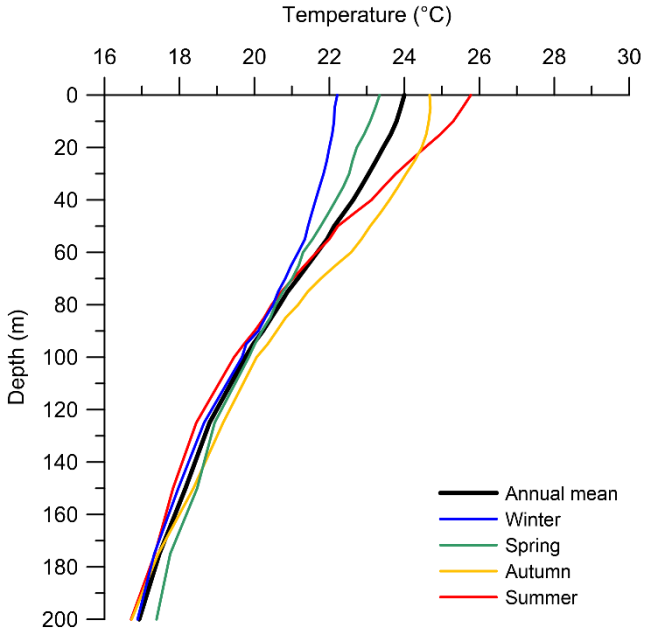

Fig. 2: Vertical profiles of the present-day temperatures in the upper 200 m of the study area provided by the World Ocean Atlas 2013 (Locarnini et al., 2013): annual mean (black), winter (blue), spring (green), autumn (yellow) and summer (red). (For interpretation of the references to color in this figure legend, the reader is referred to the web version of this article.)

3. MATERIAL AND METHODS

3.1. Sediment sampling and age model

The marine sediment core GL-1090 (24.92 °S, 42.51 °W, 2225 m water depth, 1914 cm length) was collected by Petrobras on the continental slope of the Santos Basin (Fig. 1) and stored in a refrigerated container at 4 °C. The age model, shown for the first time in Santos et al. (2017a), was based on radiocarbon dating and visual alignment of $\delta^{18}O$ from benthic foraminifera with two reference curves, MD95-4042 (Govin et al., 2014) and LR04 $\delta^{18}O$ global stack (Lisiecki and Raymo, 2005). The final age model was built using Bacon software v.2.2 (Blaauw and Christeny, 2011). Recently, Ballalai et al. (2019) and Santos et al. (2020) implemented several improvements over the original age model. Ballalai et al. (2019) chose one of the 230^{Th} ages of the Sanbao cave as the connection point for the abrupt transition observed in the corrected ice volume $\delta^{18}O$ at the end of Termination II. This modification, with assumes a coupling between the movements of the Intertropical Convergence Zone and the bifurcation of the South Equatorial Current in the tropical Atlantic, reduced age uncertainties from ± 3.87 to ± 1.51 ka close to the transition to the LIG. Santos et al. (2020) derived more benthic $\delta^{18}O$ tie- points between GL-1090 and the Iberian Margin MD95-2042 (Govin et al., 2014) on the AICC2012 time scale (Bazin et al., 2013; Veres et al., 2013). The success of the new tie-points can be seen through a precise alignment between the variability on the $\delta^{18}O$ millennial scale of *Globorotalia inflata* and NGRIP (Santos et al., 2020). Core GL-1090 spans the last 185 ka. This study is focused on the age interval from 150 to 65 ka, corresponding to the depth interval from 1591 to 689 cm. Each subsample is 2 cm thick with average collection intervals of 5 cm, corresponding to an average sampling resolution of approximately 400 years.

3.2. Lipid biomarker extraction and fractionation

Lipids were extracted from dry-frozen sediments (2 - 5 g) via three ultrasonication cycles using a solvent mixture of dichloromethane/methanol, 3:1 (v:v). The total lipid extracts were further separated into three fractions by silica gel chromatography using solvent mixtures of increasing polarity: 4 mL of hexane (elution of *n*-alkanes - not discussed in this study); 2 mL of hexane/ethyl acetate 95:5 (v:v) and then, in sequence, 2 mL of hexane/ethyl acetate 90:10 (v:v) (elution of alkenones); and 5 mL of hexane/ethyl acetate 70:30 (v:v) (elution of GDGTs).

3.3. Alkenone analysis and temperature estimations

The fractions containing alkenones were analyzed on an Agilent 6890 Plus gas chromatograph coupled with a flame ionization detector (GC-FID), and equipped with a CPSIL-5 CB column (50 m long × 0.32 mm internal diameter × 0.25 μm film thickness). Helium gas was used as carrier gas (2.0 mL/min). The oven was programmed with an initial temperature of 50 °C, which was then increased to 140 °C at 30 °C/min, then to 280 °C at 20 °C/min, and finally to 305 °C at 0.5 °C/min. Di- and tri-unsaturated C_{37} alkenones ($C_{37:2}$ and $C_{37:3}$, respectively) were quantified by comparing their peak area with that of an internal standard (5α-cholestane, added prior to analysis).

The alkenone unsaturation index $U_{37}^{K'}$ was calculated according to Prahl and Wakeham (1987; Equation 1) and converted into temperature values using the Bayesian B-spline regression model, BAYSPLINE, for the $U_{37}^{K'}$ paleothermometer (Tierney and Tingley, 2018), with a standard error of ± 1.0 °C.

$$U_{37}^{K'} = \frac{C_{37:2}}{C_{37:2} + C_{37:3}} \quad (1)$$

191 3.4. GDGT analysis and temperature estimations

192 GDGT analyses were performed on a Shimadzu LCMS-2020 high-performance liquid
193 chromatography-mass spectrometry (HPLC-MS) system, as recently described by
194 Huguet et al. (2019). The semi-quantification of the GDGTs was performed by comparing
195 the peak area of the internal standard C_{46}GDGT with those of the compounds (cf. Huguet
196 et al., 2013).

197 The TEX_{86} index was calculated according to Schouten et al. (2002) (Equation 2). The
198 numbering of the isoGDGTs refers to the publication by Kim et al. (2010).

199

200 $$TEX_{86} = \frac{\text{isoGDGT-2 + isoGDGT-3 + Crenarchaeol regioisomer}}{\text{isoGDGT-1 + isoGDGT-2 + isoGDGT-3 + Crenarchaeol regioisomer}} \quad (2)$$

201

202 The annual mean sea surface temperatures (0 m) were estimated from the TEX_{86}^{H} index
203 (Equation 3) using the calibration by Kim et al. (2010) adapted for temperatures between
204 15 – 30 °C, with a given uncertainty of ± 2.5 °C (Equation 4).

205

206 $$TEX_{86}^{H} = \log(TEX_{86}) \quad (3)$$

207

208 $$\text{Temp-}TEX_{86}^{H}\ (°C) = 68.4\ (TEX_{86}^{H}) + 38.6 \quad (4)$$

209

210 The annual mean depth-integrated temperatures (0 to 200m water depth) were
211 calculated from the global calibration by Kim et al. (2012; Equation 5), with an
212 uncertainty of ± 2.2 °C.

213

214 $$\text{Temp-}TEX_{86}^{H}(0\text{-}200)\ (°C) = 54.7\ (\ TEX_{86}^{H}) + 30.7 \quad (5)$$

215

The Branched and Isoprenoid Tetraether (BIT) index is suggested to represent terrestrial organic matter inputs into aquatic environments (Hopmans et al., 2004). In order to evaluate if TEX_{86}^{H} values were biased by terrigenous input at our core site, the BIT index was calculated from Hopmans et al. (2004) (Equation 6). The numbering of the branched GDGTs (brGDGTs) refer to the publication by Hopmans et al. (2004). High BIT values (> 0.4) may lead to anomalously high TEX_{86}^{H}-derived temperatures (Weijers et al., 2006).

$$\text{BIT index} = \frac{\text{brGDGT-I} + \text{brGDGT-II} + \text{brGDGT-III}}{\text{brGDGT-I} + \text{brGDGT-II} + \text{brGDGT-III} + \text{Crenarchaeol}} \quad (6)$$

4. RESULTS

4.1. Alkenone-derived temperatures (Temp-$U_{37}^{K'}$)

During the period between 150 and 65 ka, the mean Temp-$U_{37}^{K'}$ was 20.8 °C ± 1.4 and ranged from 17.6 °C (ca. 146.4 ka ka, MIS 6) to 26.8 °C (ca. 126.6 ka, MIS 5e) (Fig. 3a). The alkenone temperature estimates were mainly below the mean value from 150 to 140 ka (MIS 6 / T II). An abrupt warming of 6.1 °C marked the Termination II (T II), reaching a peak during MIS 5e (~127 ka), followed by a gradual cooling until mid-MIS 5d (ca. 112 ka). The MIS 5e, 5c, and 5a substages generally showed warmer temperatures than MIS 5d and 5b substages. The periods between ca. 82 - 79 ka and ca. 77 - 75 ka were marked by a decrease in temperature.

4.2. GDGT-derived temperatures (Temp-TEX_{86}^{H}, Temp-TEX_{86}^{H} (0-200)

The mean Temp-TEX_{86}^{H} from 140 to 65 ka was 25.4 ºC ± 1.4, ranging from 21.1 ºC (ca. 68.4 ka, MIS 4) to 28.5 ºC (ca. 123.8 ka, MIS 5e) (Fig. 3a). The T II was marked by an abrupt warming of 5.7 °C. Throughout the substages MIS 5d to MIS 5a, the

241 temperatures remained roughly stable, except for two abrupt decreases in temperature
242 during MIS 5a. The minimum temperature was recorded at the MIS 5a / 4 (21.1 °C at
243 69 ka). Regarding the depth-integrated temperatures, Temp-TEX_{86}^{H} (0-200) oscillated
244 between 16.7 ºC (ca. 68.4 ka, MIS 4) and 22.7 ºC (ca. 123.8 ka, MIS 5e), with an average
245 of 20.1 ºC ± 1.2 (Fig. 4).
246
247 5. DISCUSSION
248 5.1. Comparison of the TEX_{86}^{H} and $U_{37}^{K'}$ temperature estimates
249 In core GL-1090, similar trends were generally observed for temperatures derived
250 from alkenones and isoprenoid GDGTs (Temp-$U_{37}^{K'}$ and Temp-TEX_{86}^{H}), with a high
251 amplitude during LIG (Fig. 3). Nevertheless, the two organic proxies provided different
252 absolute temperature estimates. $U_{37}^{K'}$-derived temperatures were systematically lower than
253 those provided by TEX_{86}^{H} (Fig. 3a). The peaks of Temp-$U_{37}^{K'}$ and Temp-TEX_{86}^{H} were 26.8
254 °C (126.6 ka, MIS 5e) and 28.5 °C (123.8 ka, MIS 5e), respectively, which are 2.8 °C and
255 4.5 °C higher than the current annual mean surface temperature (0 m depth) near the GL-
256 1090 site (Fig. 3a).
257 Turney and Jones (2010) compiled a global dataset of annual temperatures from cores
258 spanning the LIG and deduced an increase in sea surface and terrestrial temperatures of
259 nearly 2.0 °C above pre-industrial levels over this period. However, such warming was
260 not uniform across the global oceans, and the SSWA was not included in the dataset.
261 Model data performed by Otto-Bliesner et al. (2013) and sea surface temperature
262 reconstructions published by Hoffman et al. (2017) did not indicate a significant
263 difference in temperature during the LIG compared with the present in global tropical
264 regions. It should be noted that these authors did not present results near our sampling
265 site.

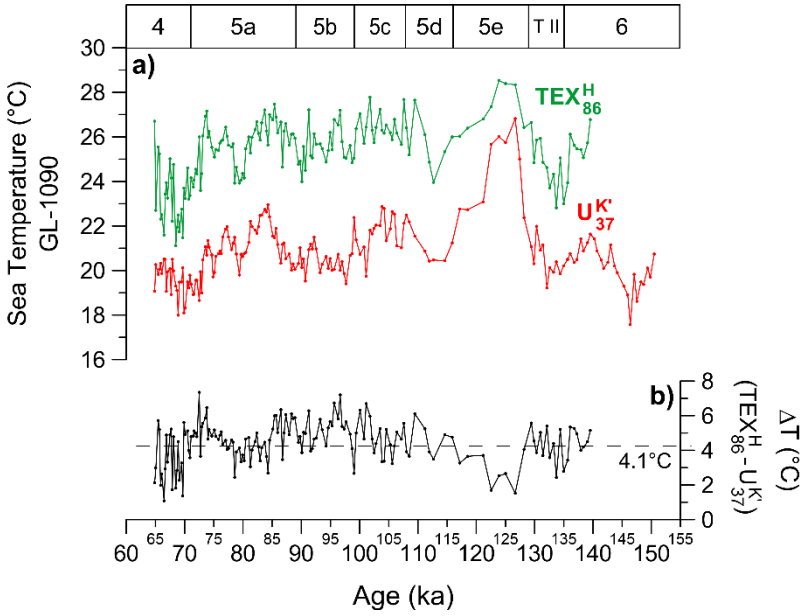

Fig. 3: Comparison of paleotemperatures reconstructed from isoGDGTs and alkenones: a) Temp-TEX_{86}^{H} (green) and Temp-$U_{37}^{K'}$ (red). The dashed line in violet marks the global average increase during the LIG, approximately 2.0 °C relative to pre-industrial levels (Turney and Jones, 2010). The blue dashed line marks the current annual mean sea surface temperature in the study area (Locarnini et al., 2013); b) Temperature gradient ΔT (TEX_{86}^{H} - $U_{37}^{K'}$). The black dashed line marks the average ΔT (4.1 °C). The marine isotopic stages (MIS) are highlighted on the upper x-axis. (For interpretation of the references to color in this figure legend, the reader is referred to the web version of this article.)

The peak of Temp-$U_{37}^{K'}$ from GL-1090 is consistent with the + 2.0 °C LIG surface temperature anomaly relative to the present-day mean (Turney and Jones, 2010), equivalent to 24 °C in the study area (Cordeiro et al., 2014; Locarnini et al., 2013). In contrast, Temp-TEX_{86}^{H} showed a very high LIG SST anomaly relative to the modern annual mean (4.5 °C), which does not seem plausible. In order to understand the similarities and divergences between the temperature estimates derived from $U_{37}^{K'}$ and

283 TEX_{86}^{H}, the different factors which may influence these organic proxies and their
284 associated temperatures – choice of calibration equations, continental inputs, lateral
285 transport of the alkenones and isoGDGTs, ecology and seasonality of the source
286 organisms of these lipids – will be considered in detail below.
287
288 5.2. Potential factors influencing the $U_{37}^{K'}$ and TEX_{86}^{H} temperature estimates
289 5.2.1. Choice of the calibrations
290 The choice of the calibration has an influence on the absolute temperature estimates.
291 We tested the Temp-$U_{37}^{K'}$ annual calibration for the global ocean from 60 °N to 60 °S
292 (Müller et al., 1998), the Temp-$U_{37}^{K'}$ SE Atlantic annual mean core top calibration (Müller
293 et al., 1998) and the new Bayesian B-spline regression model, BAYSPLINE, for the $U_{37}^{K'}$
294 paleothermometer (Tierney and Tingley, 2018). The three calibrations resulted in highly
295 similar temperatures (cf. Supp. Fig. 1). The annual calibration for the global ocean from
296 60 °N to 60 °S resulted in Temp-$U_{37}^{K'}$ on average 0.8 °C warmer than the values obtained
297 with the SE Atlantic annual calibration equation proposed by Müller et al. (1998). The
298 Temp-$U_{37}^{K'}$ calibration by Tierney and Tingley (2018) resulted in Temp-$U_{37}^{K'}$ on average
299 0.04 °C warmer than the values calculated with the SE Atlantic annual calibration
300 equation proposed by Müller et al. (1998).
301 Using 53 core-top sediments, Ceccopieri et al. (2018) tested on a regional scale in the
302 SSWA (SE Brazilian continental margin) the applicability of Temp-$U_{37}^{K'}$ calibrations by
303 Müller et al. (1998) for the SE Atlantic: annual mean core top calibration (for
304 temperatures from 0 to 27 °C) and seasonal (austral) calibrations. These authors
305 concluded that the Temp-$U_{37}^{K'}$ SE Atlantic annual calibration (Müller et al., 1998) is
306 comparable to SSWA annual mean present-day temperatures. Due to the high similarity
307 between the Temp-$U_{37}^{K'}$ SE Atlantic annual mean core top calibration (Müller et al., 1998)

and Temp-$U^{K'}_{37}$ calibration by Tierney and Tingley (2018), both calibrations could be used interchangeably. In this work we adopt the most recent one.

Regarding GDGTs, we tested the Temp-TEX^{H}_{86} calibration proposed by Kim et al. (2010), the Temp-TEX^{H}_{86}(0-200) calibration by Kim et al. (2012), and the Temp-TEX^{H}_{86} and Temp-TEX^{H}_{86}(0-200) calibrations by Tierney and Tingley (2014). The TEX^{H}_{86} and TEX^{H}_{86} (0-200) calibrations by Tierney and Tingley (2014) resulted in a less pronounced temperature oscillation over time, and the absolute surface and subsurface values were closer to each other (cf. Supp. Fig. 2). The TEX^{H}_{86} calibration by Tierney and Tingley (2014) resulted in colder absolute temperatures than the TEX^{H}_{86} calibration by Kim et al. (2010). The TEX^{H}_{86} (0-200) calibration by Tierney and Tingley (2014) resulted in warmer absolute temperatures than the TEX^{H}_{86} (0-200) calibration by Kim et al. (2012).

The applicability of the Temp-TEX^{H}_{86} calibration for regions with present-day temperatures from 15 to 30 °C proposed by Kim et al. (2010) was also tested by Ceccopieri et al. (2018) in the SSWA using the same core-top sediments as for the $U^{K'}_{37}$ investigation. Temp-TEX^{H}_{86} was found to reflect the annual temperature in the SSWA. Although the Temp-TEX^{H}_{86} by Tierney and Tingley (2014) are closer to the present-day temperature in GL-1090, we adopted Kim et al. (2010) calibration because its regional application in our study area was already validated by previous study.

5.2.2. Continental inputs

Temp-TEX^{H}_{86} may be biased by isoprenoid GDGTs derived from terrigenous inputs and transported to the marine system by rivers and/or runoff (Schouten et al., 2013 and references therein). These inputs can notably be quantified by applying the BIT index (Hopmans et al., 2004), whose values close to 0 were generally associated with organic

material from open sea origin and those close to 1 (maximum value) with organic matter from terrestrial origin. In marine settings, BIT values above 0.4 were suggested to cause a deviation of the TEX_{86} temperature estimates greater than 2.0 °C (Weijers et al., 2006). Nevertheless, care should be taken when interpreting the BIT values, as the two types of GDGTs used to calculate the BIT index - branched glycerol dialkyl glycerol tetraethers (brGDGTs) (Peterse et al., 2009; Sinninghe Damsté et al., 2009; Tierney et al., 2010) and crenarchaeol (Leininger et al., 2006; Weijers et al., 2006; Walsh et al., 2008) - can be produced in both terrestrial and aquatic environments. Therefore, in aquatic settings, high BIT values, which reflect a higher relative abundance of brGDGTs than that of crenarchaeol, could be associated with high terrestrial inputs of brGDGTs and/or *in situ* production of brGDGTs.

Along the core GL-1090, the BIT index varied between 0.11 and 0.92, with an average of 0.45 ± 0.12 and higher values recorded during cold periods, from late MIS 6 to the onset of MIS 5e and during the onset of MIS 4 (cf. Supp. Fig. 3). Considering that previous studies have shown that no large river flows directly to the sea in this region (Conti and Furtado, 2006; Pessenda et al., 2012), terrestrial inputs were not expected to be high in the study area. To better evaluate this hypothesis, the behavior of organic and inorganic compounds from the same core was investigated, even though the latter are transported from the continent to marine sediments by different particles. No similar trends were observed between the BIT values and the Fe/Ca ratio - an inorganic proxy from continental runoff along the GL-1090 core (Figueiredo et al., 2020). The Fe/Ca peaks were not even registered by the BIT index or by Temp-TEX_{86}^{H} (cf. Supp. Fig. 3).

However, the calcium ratios are influenced by sea level in the study area, embedding a very dominant low-frequency variability in the data. This sea level influence may suggest that the null correlation between BIT and XRF may not be substantially strong

evidence. Recently, Mathias et al. (2021) performed a deep sedimentological analysis on GL-1090 and they found very little river entry into the continental margin of southeastern Brazil during the Late Pleistocene. Although there was some continental influence, the results indicated the lowest terrigenous entries during MIS 5e and MIS 1. This suggests that the BIT values cannot be interpreted as recording high terrestrial inputs, since its highest values were found during MIS 5e. The high BIT values would rather be due to *in situ* production of brGDGTs at the GL-1090 sampling site, as observed in coastal regions (Crampton-Flood et al., 2019).

5.2.3. Lateral transport

The effect of lateral transport on $U^{K'}_{37}$ temperature estimates has been reported in specific oceanic regions. Anomalously cold (by 2 °C – 6 °C) $U^{K'}_{37}$ temperature values were found in sediments located under the Brazil–Malvinas Confluence and Malvinas Current in the southwestern Atlantic (Benthien and Muller, 2000). In this area of peculiar circulation, alkenone-bearing sediments are advected northwards carrying $U^{K'}_{37}$ signals of their origin in cold waters. In the Campos Basin, SSWA, cold bias in Uk'37 derived temperatures wre reported in core-top sediments close to the Cabo Frio Upwelling System and they were ascribed to alkenones advected from adjacent colder (upwelled) waters.

Considering that alkenones are more susceptible to lateral transport than isoGDGTs (Mollenhauer et al., 2007; Shah et al., 2008), Ceccopieri et al. (2018) suggested that TEX^{H}_{86}–derived estimates better reflect local temperatures in this region in comparison with alkenones. In line with the conclusion of Ceccopieri et al. (2018), the lower absolute values of $U^{K'}_{37}$ compared with those of TEX^{H}_{86} could be explained by intrusions of SACW into the photic zone identified in the GL-1090 during MIS 5e, 5c, and 5a substages due to the southward expansion of the Cabo Frio Upwelling System (Lessa et al. 2017).

382 Nevertheless, it should be noted that, while Lessa et al (2017) showed a vertical cooling
383 only during warm substages, here Temp-$U^{K'}_{37}$ presented lower values than Temp-
384 TEX^{H}_{86} during the entire studied period (150 – 65 ka), indicating that the advection of cold
385 water alone cannot explain the differences in TEX^{H}_{86} and $U^{K'}_{37}$-based temperature
386 estimates. Additionally, the similar pattern and the high correlation between temperatures
387 derived from the $U^{K'}_{37}$ and TEX^{H}_{86} indices ($r = 0.73$, $p < 0.05$) suggest that either (i) the
388 signals from the alkenones and isoGDGTs were produced vertically in the same area,
389 probably at different depths in the water column, or (ii) the intensity of the lateral
390 transport might differ over the investigated period, affecting both types of lipids in the
391 same way during some periods. In any case, it means that lateral transport alone cannot
392 explain the differences in absolute temperatures between $U^{K'}_{37}$ and TEX^{H}_{86}.
393
394 5.2.4. Seasonality
395 In a number of studies disparities between paleotemperatures reconstructed with the
396 $U^{K'}_{37}$ and TEX^{H}_{86} indexes have been attributed to seasonal patterns in the production of the
397 organisms, hapophyte algae and marine Thaumarchaeota, respectively (eg Lopes dos
398 Santos et al., 2013; Auderset et al., 2019) but a consistent, globally applicable, seasonal
399 pattern has not emerged.
400 Furthermore, compilation of sediment trap time series data have shown that the
401 maximum alkenone flux across the oceans displays seasonal variations depending on
402 local/regional oceanographic conditions and sedimentation processes (Mele and Prahl
403 2013). However, apart from few locations close to major hydrographic fronts,
404 sedimentation patterns for $U^{K'}_{37}$ in sediment trap time series appears provide a measure of
405 annual mean SST.

406 The age of the GL-1090 core-top sample is 6.6 ka (Santos et al., 2017a), hampering
407 its use to compare the seasonality of alkenone and isoGDGT source organisms -
408 hapophyte algae and marine *Thaumarchaeota*, respectively - in the present-day.
409 However, core-top studies in the SSWA shelf and slope (Cordeiro et al., 2014; Ceccopieri
410 et al., 2018) have found that $U^{K'}_{37}$-derived temperature estimates agreed well with
411 interpolated mean annual SST of ca. 24 °C. They also reported that, despite a likely most
412 efficient export of isoGDGT during austral summer, core-top Temp-TEX^{H}_{86} values were
413 better correlated with the annual mean SST (Ceccopieri et al., 2018). In the regional
414 context, Mahiques et al. (2005) analyzed alkenones in box cores near GL-1090 and
415 considered Temp-$U^{K'}_{37}$ as reflecting mean annual temperatures over the last 700 years. A
416 similar conclusion was drawn by Dauner et al. (2019), who showed that the temperature
417 estimates derived from TEX^{H}_{86} and $U^{K'}_{37}$ over the last 75 ka reflected the mean annual
418 temperature in the SSWA.
419 Based on the afore-mentioned studies we argue that seasonal bias in the Temp-TEX^{H}_{86}
420 and Temp-$U^{K'}_{37}$ estimates is of minor importance and that both TEX^{H}_{86} and $U^{K'}_{37}$ indexes
421 record the mean annual temperature in the study area.
422
423 5.2.5. Water depth
424 Standard deviations of ± 1.0 °C for Temp-$U^{K'}_{37}$ (Müller et al., 1998) and ± 2.5 °C for
425 Temp-TEX^{H}_{86} (Kim et al., 2010) suggest that temperature differences of up to ± 3.5 °C
426 between these proxies may be within the calibration error. The reconstructed mean
427 temperature gradient (ΔT) of TEX^{H}_{86} and $U^{K'}_{37}$ is 4.5 °C (Fig. 3b) and, therefore, higher
428 than the calibration error. One explanation may be the difference of depth production
429 between haptophytes and *Thaumarchaeota*.

Previous studies at the Campos Basin slope indicate that haptophyte algae, alkenone producers, inhabit the photic zone between 6 – 50 m depth (predominantly the 20 °C isotherm; Mahiques et al., 2009; Sousa et al., 2014; Rodrigues et al., 2014). This temperature isotherm corresponds to the interface between TW and SACW at the Santos Basin slope. Dauner et al. (2019) concluded that the temperatures derived from $U^{K'}_{37}$ were consistent with those at around 30 m depth in the SSWA. Similarly, Luz (2019) considered that the $U^{K'}_{37}$ signal reflected the temperature of the water column up to 25 m in the same region. This is consistent with previous studies in other areas, such as the Mediterranean Sea, the northern Arabian Sea, and in the tropical and subtropical Atlantic Ocean, which reported the possibility of alkenones recording temperature conditions below the surface (Ternois et al., 1997; Andruleit et al., 2003; Poulton et al., 2017).

IsoGDGT-producing archea are generally more widely distributed in the water column than haptophytes, presenting a greater abundance between 40 and 150 m water depth (Lopes dos Santos et al., 2013; Kim et al., 2012; Schouten et al., 2002; Wuchter et al., 2006). In their study of the structure of the picoplankton community in a southern Atlantic transect, Zubkov et al. (2000) indicated that heterotrophic prokaryotes (bacteria and archea) mainly inhabit the surface layer. While Dauner et al. (2019) confirmed that the TEX^{H}_{86} signal represents the average annual temperature of the surface layer at the Santos Basin, Luz (2019) considered that Temp-TEX^{H}_{86} reflects those of the water depths around 100 - 200m, showing that there is no consensus on the depth of *Thaumarchaeota* growth in the SSWA.

Assuming that the non-thermal factors investigated in the previous sections (5.2.1, 5.2.2, 5.2.3 and 5.2.4) do not cause significant deviations in temperature reconstructions, the results for the GL-1090 core suggest that the alkenones reflect temperatures at the

interface between the TW and the SACW, corresponding to the upper thermocline, and the isoGDGTs reflect temperatures at the mixed layer of the Santos Basin slope.

5.3. Multiproxy temperature reconstruction in the water column

In order to estimate the temperature gradient (ΔT) between the mixed layer and the upper thermocline from GL-1090, Temp-TEX^{H}_{86}(0-200) – for subsurface temperature – was calculated and compared with Temp-TEX^{H}_{86} – for surface temperature. The average ΔT between Temp-TEX^{H}_{86} and Temp-TEX^{H}_{86}(0-200) was 5.2 °C (Fig. 4a), while the average ΔT between Temp-TEX^{H}_{86}(0-200) and Temp-$U^{K'}_{37}$ was considerably smaller (less than 1.0 °C) (Fig. 4b).

Ceccopieri et al. (2018) also applied the Temp-TEX^{H}_{86}(0-200) calibration by Kim et al. (2012) to core-top samples. At station A11 (Fig. 1b,c), these authors obtained values close to instrumental data from WOA13 (Locarnini et al., 2013) depth-integrated temperatures at about 100 - 200 m depth throughout the Campos Basin slope (between 13.8 °C and 21.7 °C). This suggests that the $U^{K'}_{37}$ signal at the GL-1090 site reflects the upper thermocline temperature in the SSWA.

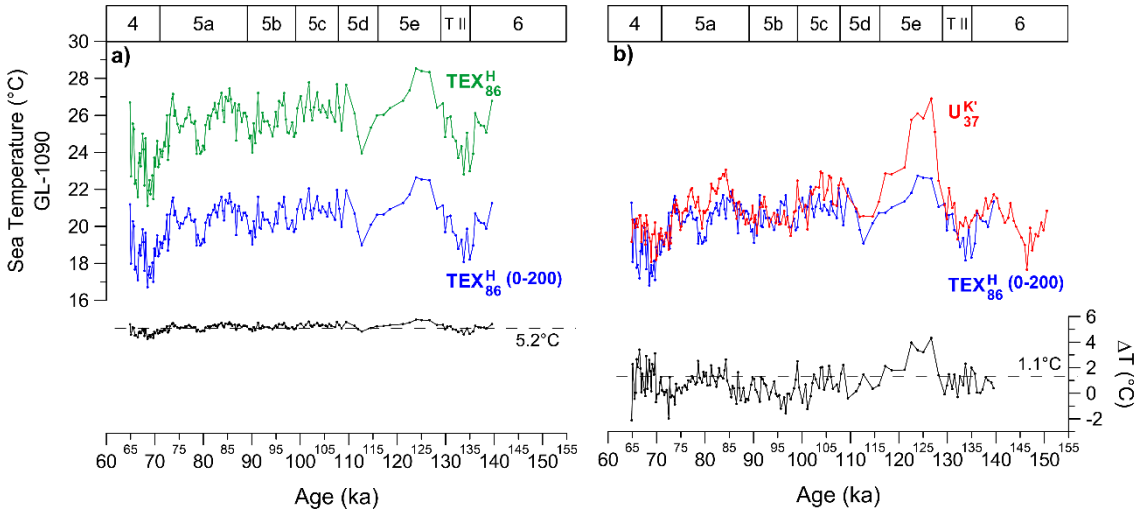

Fig. 4: Comparison of depth-integrated TEX_{86}^{H}(0-200) with TEX_{86}^{H} and $U_{37}^{K'}$-based temperatures, and their respective temperature gradients: a) TEX_{86}^{H} (green), TEX_{86}^{H}(0-200) (blue) and ΔT (TEX_{86}^{H}-TEX_{86}^{H}(0-200)) (black); b) $U_{37}^{K'}$ (red), TEX_{86}^{H}(0-200) (blue) and ΔT ($U_{37}^{K'}$-TEX_{86}^{H}(0-200)) (black). Dashed lines mark the mean difference between the absolute temperatures derived from the organic proxies. Marine isotope stages (MIS) are highlighted on the upper x-axis. (For interpretation of the references to color in this figure legend, the reader is referred to the web version of this article.)

The sea temperature estimates derived from $U_{37}^{K'}$ and TEX_{86}^{H} were compared with those inferred for the same core from Mg/Ca *G. ruber* (Santos et al., 2017a) and from Modern Analog Technique (MAT) - a transfer function based on planktonic foraminiferal census count (Lessa et al., 2017) - at 10m (MAT-10m) and at 100m (MAT-100m) water depth. The Mg/Ca values published in Santos et al. (2017a) were converted to temperatures using the recent species-specific equation by Gray and Evans (2019). The calcification depth of *G. ruber* in the SSWA corresponds to the mixed layer (30 – 40m water depth), as shown by sediment traps studies (Venancio et al., 2017). This supports the use of the Mg/Ca proxy for reconstructing mixed layer temperatures in the region (eg Chiessi et al., 2007; Chiessi et al. 2014). Temp-TEX_{86}^{H} values fall into the range of those derived from Mg/Ca and are close to MAT-10m temperatures, suggesting that these proxies reflect mixed layer temperatures (Fig. 5a).

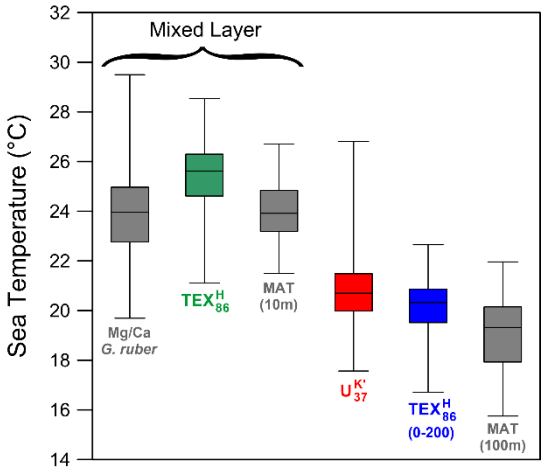

Fig. 5: Comparison of paleotemperature ranges reconstructed from multiproxies at GL-1090, between 150 and 65 ka: temperature (°C) derived from Mg/Ca *G. ruber* (gray) (after Santos et al., 2017a); TEX_{86}^{H} (green) (this study); MAT-10m (gray) (Lessa et al., 2017); $U_{37}^{K'}$ (red) (this study); TEX_{86}^{H}(0-200) (blue) (this study); and MAT-100m (gray) (Lessa et al., 2017). (For interpretation of the references to color in this figure legend, the reader is referred to the web version of this article.)

In contrast, the range of temperatures derived from $U_{37}^{K'}$ is similar to the ones from TEX_{86}^{H}(0-200) and MAT-100 m. The corresponding estimates are lower than Mg/Ca, TEX_{86}^{H} and MAT-10m-based temperatures, suggesting that, in core GL-1090, Temp-$U_{37}^{K'}$ recorded temperatures from the upper thermocline. This is consistent with the fact that, in the SSWA, haptophytes reach their maximum abundance where the deep chlorophyll maximum occurs, above the thermocline (Brandini et al., 2014; Rodrigues et al., 2014; Ribeiro et al., 2016). Dauner et al. (2019) also attributed to the depth of the haptophyte habitat the lower Temp-$U_{37}^{K'}$ than Temp-TEX_{86}^{H} over the last 75 ka in the SSWA, and this condition seems to be the most likely to explain why the temperatures derived from $U_{37}^{K'}$ are more similar to the temperatures from the upper thermocline than from the mixed layer in GL-1090, between 150 and 65 ka (Fig. 5b).

5.4. Regional dynamics in the water column in the SSWA during MIS 5e

During the MIS 5e (129-116 ka) and the onset of MIS 4 (71-65 ka), the ΔT between TEX_{86}^{H} and $U_{37}^{K'}$ was lower than the average one over the whole core GL-1090 (Fig. 3b). During the MIS 5e, the ΔT was reduced due to a more prominent warming of $U_{37}^{K'}$. In contrast, during the onset of the MIS 4, this decrease could be explained by a more pronounced cooling of TEX_{86}^{H}. If we assume that the source organisms of alkenones and isoGDGTs live at different depths, then a change in the thermal structure of the photic zone may explain the similar temperatures between the mixed layers and the upper thermocline during MIS 5e and the onset of MIS 4. The pronounced positive temperature anomaly derived from $U_{37}^{K'}$ during MIS 5e (Fig. 6a) suggests greater heat storage at the upper thermocline.

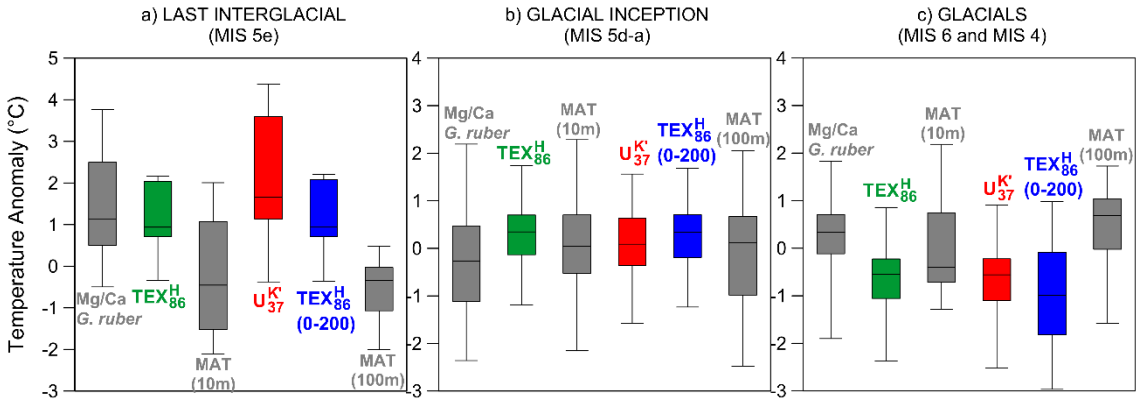

Fig. 6: Temperature anomalies normalized by the standard deviation of each proxy along the core GL-1090 for three time intervals: (a) Last Interglacial (LIG/MIS 5e); (b) Glacial inception (MIS 5d-a); (c) Glacials (MIS 6 and MIS 4), based on Mg/Ca *G. ruber* (gray) (after Santos et al., 2017a); TEX_{86}^{H} (green) (this study); MAT-10m (gray) (Lessa et al., 2017); $U_{37}^{K'}$ (red) (this study); TEX_{86}^{H}(0-200) (blue) (this study); and MAT-100m (gray)

(Lessa et al., 2017). (For interpretation of the references to color in this figure legend, the reader is referred to the web version of this article.)

During the LIG period (Figure 6a), $U^{K'}_{37}$ recorded a steep thermal gradient in the upper thermocline, which decreased in the middle/end of the interglacial complex scenario (Figure 6b). The intensity of this thermal gradient was further reduced in the glacial scenario (Figure 6c). The evaluation of these different water column temperature profiles over time suggests that alkenones are more strongly affected by changes in depth conditions than isoGDGTs, the latter being directly affected by the vertical mixing temperature oscillation. This explains why $U^{K'}_{37}$-based temperatures are similar to those of the surface layer during the LIG and close to the subsurface temperatures during the glacials.

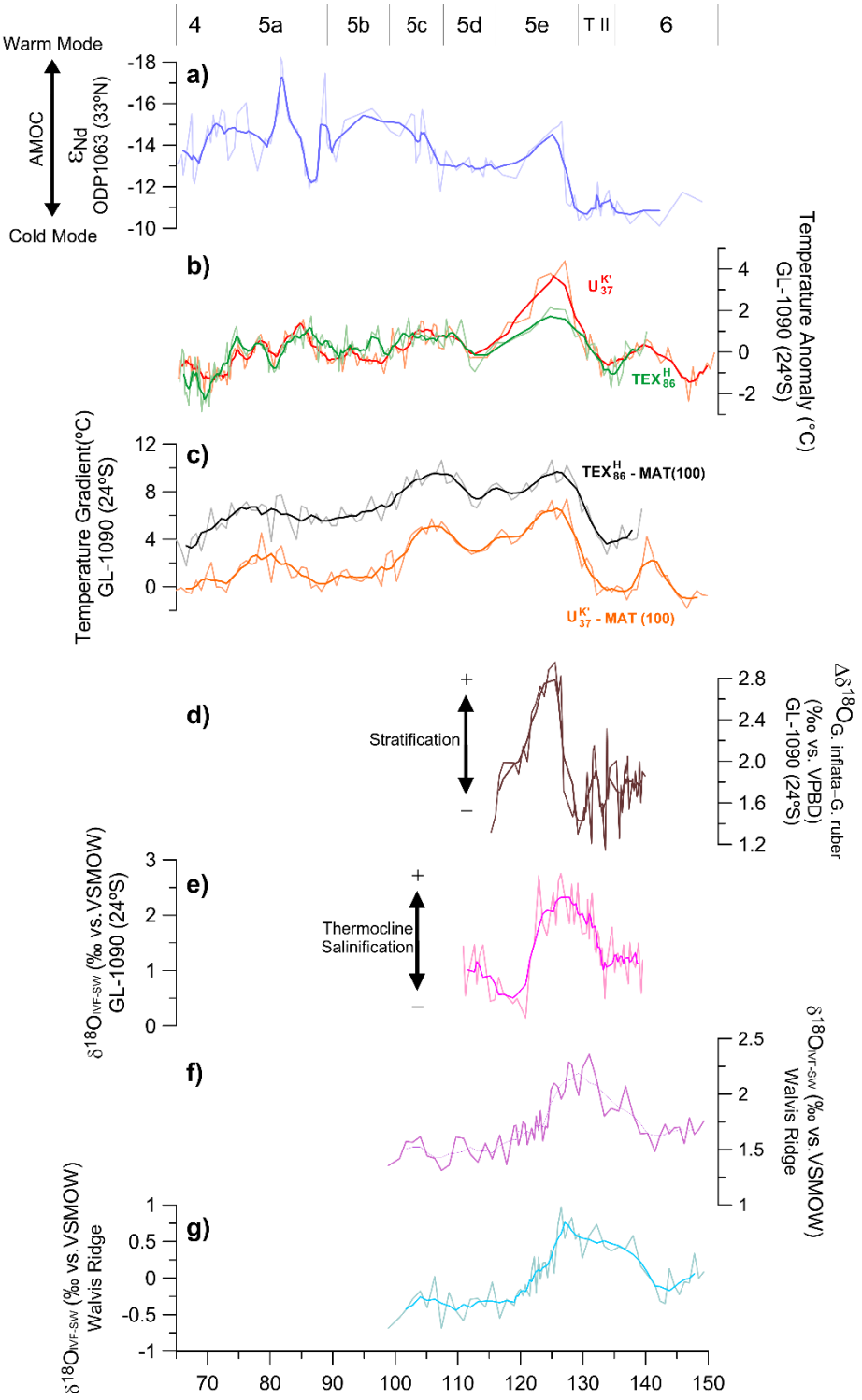

Figure 7: Comparison of temperature anomalies from core GL-1090 with other low/mid-paleoclimate signals from 150 to 65 ka: a) εNd record of core ODP1063 (Böhm et al., 2015); b) Temperature anomalies from core GL-1090 based on TEX_{86}^{H} (green) and $U_{37}^{K'}$ (red) (this study); c) Temperature gradient from core GL-1090 based on TEX_{86}^{H} (this study) minus MAT-100m (Lessa et al., 2017; green), and $U_{37}^{K'}$ (this study) minus MAT-100m (Lessa et al., 2017; red); d) $\Delta\delta^{18}O$ (*Globorotalia inflata* – *Globigerinoides ruber*) (Santos et al.,

2017); e) Thermocline $\delta^{18}O_{IVC\text{-}SW}$ values from core GL-1090 (Ballalai et al., 2019) estimated from Mg/Ca ratio-derived thermocline temperatures; f) Surface $\delta^{18}O_{IVC\text{-}SW}$ values from core 64PE- 174P13 (Walvis Ridge) (Scussolini et al., 2015) estimated from *Globigerinoides ruber* $\delta^{18}O$ values; g) Thermocline $\delta^{18}O_{IVC\text{-}SW}$ values from core 64PE-174P13 (Walvis Ridge) (Scussolini et al., 2015) estimated from *Globigerinoides truncatulinoides* $\delta^{18}O$ values. Marine isotope stages (MIS) are highlighted on the upper x-axis. (For interpretation of the references to color in this figure legend, the reader is referred to the web version of this article.)

Furthermore, during MIS 5e and MIS 5c, the high ΔT between the organic proxies $U^{K'}_{37}$/TEX^{H}_{86} and MAT-100 (Fig. 7) suggests upper ocean stratification with the flattening of the mixed layer, which may have reduced the downward diffusion of heat. This decrease in vertical mixing due to enhanced stratification is showed by $\Delta\delta^{18}O$ (*G. inflata* - *G. ruber*) (Fig. 7d). Leonhardt et al. (2013) analyzed fossil assemblages of coccolithophorids, *Globigerinoides ruber* and corresponding stable oxygen isotopes from a sediment core collected in the SSWA, covering the last 130 ka. The authors observed lower surface productivity during MIS 5e, which was related to an increase in the nutricline depth, making surface water fertilization impossible.

During late MIS 6 / T II and the onset of MIS 4, sea temperature positive anomalies (Fig. 7b) were associated with the weakening of the AMOC and consequent strengthening of the BC due to changes in circulation structure (Broecker, 1998; Santos et al., 2017). The εNd, a water mass provenance proxy used for interpretation of water mass geometry from the Bermuda Rise (Böhm et al., 2015), corroborates this hypothesis (Fig. 7a).

It is known that warm and saline Subtropical Indian Ocean water is transported into the South Atlantic through the Indian-Atlantic oceanic gateway (Gordon, 1986; Lutjeharms, 2006; Beal et al., 2011). Marino et al. (2013) point that the salinity increase between 138 ka and 130 ka indicated by $\delta^{18}O_{SW}$ represents an interhemispheric coupling

578 once it is correlated with abrupt swings in the North Atlantic. According to Marino et al.
579 (2013), the Indian-to-Atlantic salt transport is a strong driver of the AMOC during the
580 abrupt climate changes of the Late Pleistocene.

581 Ballalai et al. (2019) analyzed thermocline Mg/Ca-derived temperatures and salinity
582 from ice volume-corrected $\delta^{18}O$ seawater ($\delta^{18}O_{IVC\text{-}SW}$) records in GL-1090 during
583 Termination II and early Late Interglacial (Fig. 7e). According to these authors, during
584 the intensification of the Agulhas Leakage, starting from ca. 142 ka BP (Fig. 7f; g), the
585 salt anomaly was recirculated within the South Atlantic subtropical gyre instead of being
586 immediately transmitted to the North Atlantic due to a "barrier" caused by an ocean-
587 atmosphere coupling that increased the BC flow and limited its equatorial crossing. Our
588 findings are consistent with those of Ballalai et al. (2019). In this sense, this study confirm
589 the connection between the intensification of the Agulhas Leakage and the heat storage
590 at the upper thermocline in the SSWA during MIS 5e.

591 In summary, our organic data from GL-1090 provided information on the applicability
592 of the $U_{37}^{K'}$ and TEX_{86}^{H} proxies in the SSWA and have enabled the identification of a
593 change in the thermocline structure in the SSWA from late MIS 6 to the onset of MIS 4.
594 Based on our results, we suggest that alkenones were more affected by warm temperatures
595 at the upper thermocline during the LIG period (MIS 5e), and isoGDGTs were more
596 affected by cold temperatures at the mixed layer during glacials (MIS 6 and MIS 4).
597 However, more studies covering the same time range with atmospheric modeling and
598 thermocline proxies in the South Atlantic must be considered in future research studies
599 in the region in order to better understand the mechanisms that led to these scenarios.
600

601 ## 6. CONCLUSIONS

This work presents the first temperature reconstruction based on alkenones and isoGDGTs covering late MIS 6 to the onset of MIS 4 in the SSWA. A multiproxy approach was developed, involving the organic proxies $U^{K'}_{37}$ and TEX^{H}_{86}, as well as previously published data (Mg/Ca ratio and MAT derived from planktonic foraminifera). Non-thermal factors, i.e. terrestrial inputs and lateral transport, were suggested to have minor influence on the temperature signal derived from alkenones/isoGDGTs. TEX^{H}_{86} and $U^{K'}_{37}$ temperature estimates were assumed to reflect different water depths, i.e. those of the mixed layer and the upper thermocline, respectively. This was related to the different habitat depths of the source organisms of isoGDGTs and alkenones - marine *Thaumarchaeota* and hapophyte algae, respectively.

Our downcore record emphasizes the relevance of a multiproxy approach to bringing insights into the interpretation of the response of each proxy in the same sediment core, leading to better understanding of the paleoceanographic changes from 150 ka to 65 ka, mainly during the LIG, in the south-eastern Brazilian margin. Our results suggest that a steep thermal gradient in the upper thermocline exists during the LIG, as does a reduced thermal gradient in the glacial scenario. Finally, our study demonstrates that the organic proxies applied here are reliable for reconstructing paleoceanographic changes in the SSWA.

CRediT AUTHORSHIP CONTRIBUTION STATEMENT

Joana F. Cruz: writing – original draft, formal analysis, conceptualization. Alice M. S. Rodrigues, Thiago P. Santos, Igor M. Venancio, Douglas Lessa, Rodrigo L. Sobrinho, Rodrigo A. Nascimento: writing – review & editing. Ioanna Bouloubassi, Arnaud Huguet: formal analysis, review & editing. Marcelo C. Bernardes: supervision, formal analysis, review & editing.

627

628 DECLARATION OF COMPETING INTEREST

629 The authors declare that they have no known competing financial interests or personal
630 relationships that could have appeared to influence the work reported in this paper.

631

632 ACKNOWLEDGEMENTS

633 We thank Petrobras for providing the sediment core used in this research, and Vincent
634 Klein (LOCEAN-Sorbonne Université) and Christelle Anquetil (METIS-Sorbonne
635 Université) for their support during the analyses. This study was supported by
636 CAPES/Paleoceano Project (23038.001417/2014-7), CAPES-IODP/Aspecto Project
637 (88887.091731/2014-01), Project CLIMATE/Print-CAPES (88887.310301/2018-00)
638 and Finance Code 001, INSU-CNRS program LEFE (BARISTA project) and partially by
639 CNPq Project 429767/2018-8. Joana F. Cruz thank for her CNPq (140443/2016-9) and
640 CAPES/Programas Estratégicos (88881.145911/2017-01) support. This study was
641 financed in part by CNPq Project RAiN (grant 406322/2018-0). This study was also
642 funded by FAPERJ (SEI-260003/000677/2023), which currently financially supports
643 Igor M. Venancio with a JCNE grant (200.120/2023 – 281226).

644

645 REFERENCES

646 Andruleit, H., Stager, S., Rogalla, U., Cepek, P., 2003. Living coccolithophores in the
647 northern Arabian Sea: ecological tolerances and environmental control, Mar.
648 Micropaleontol., 49, 157-181, https://doi.org/10.1016/S0377-8398(03)00049-5.

649 Auderset, A., Martínez-García, A., Tiedemann, R., Hasenfratz, A.P., Eglinton, T.I.,
650 Schiebel, R., Sigman, D.M., Haug, G.H., 2019. Gulf Stream intensification after the early

651 Pliocene shoaling of the Central American Seaway, Earth Planet. Sci. Lett., 520, 268–
652 278, https://doi.org/10.1016/j.epsl.2019.05.022.

653 Ausín, B., Magill, C., Haghipour, N., Fernández, Á., Wacker, L., Hodell, D., Baumann,
654 K.-H., Eglinton, T.I., 2019. (In)coherent multiproxy signals in marine sediments:
655 Implications for high-resolution paleoclimate reconstruction, Earth Planet. Sci. Lett., 515,
656 38–46, https://doi.org/10.1016/j.epsl.2019.03.003.

657 Ballalai, J.M., Santos, T.P., Lessa, D.O., Venancio, I.M., Chiessi, C.M., Johnstone,
658 H.J.H., Kuhnert, H., Claudio, M.R., Toledo, F., Costa, K.B., Albuquerque, A.L.S. 2019.
659 Tracking spread of the Agulhas leakage into the western South atlantic and its northward
660 transmission during the last interglacial. Paleoceanog. and Paleoclimatol., [s. l.], v. 34, n.
661 11, p. 1744-1760, doi: 10.1029/2019PA003653.

662 Bazin, L., Landais, A., Lemieux-Dudon, B., Toyé Mahamadou Kele, H., Veres, D.,
663 Parrenin, F., Martinerie, P., Ritz, C., Capron, E., Lipenkov, V.Y., Loutre, M.-F.; Raynaud,
664 D., Vinther, B.M., Svensson, A.M., Rasmussen, S.O., Severi, M., Blunier, T.,
665 Leuenberger, M.C., Fischer, H., Masson-Delmotte, V., Chappellaz, J.A., Wolff, E.W.
666 2013. An optimized multi-proxy, multi-site Antarctic ice and gas orbital chronology
667 (AICC2012): 120-800 ka. Climate of the Past, [s. l.], v. 9, n. 4, 1715-1731,
668 https://doi.org/10.5194/cp-9-1715-2013.

669 Beal, L.M., De Ruijter, W.P.M., Biastoch, A., Zahn, R., 2011. On the role of the Agulhas
670 system in ocean circulation and climate, Nature, 472 (7344), 429–436.,
671 https://doi.org/10.1038/nature09983.

672 Benthien, A., Müller, P.J., 2000. Anomalously low alkenone temperatures caused by
673 lateral particle and sediment transport in the Malvinas Current region, western Argentine

674 Basin, Deep-Sea Res. Part I Oceanogr. Res. Pap., 47, 2369–2393,
675 https://doi.org/10.1016/S0967-0637(00)00030-3.

676 Blaauw, M., Christeny, J.A., 2011. Flexible paleoclimate age-depth models using an
677 autoregressive gamma process, Bayesian Anal., 6, 457–474, doi:10.1214/11-BA618.

678 Böhm, E.; Lippold, J.; Gutjahr, M.; et al, 2015. Strong and deep Atlantic meridional
679 overturning circulation during the last glacial cycle. Nature, v. 517, n. 7534, p. 73–76.

680 Brandini, F.P., Nogueira Jr, M., Simião, M., Codina, J.C.U., Noernberg, M.A., 2014.
681 Deep chlorophyll maximum and plankton community response to oceanic bottom
682 intrusions on the continental shelf in the South Brazilian Bight, Cont. Shelf Res., 89, 61–
683 75, https://doi.org/10.1016/j.csr.2013.08.002.

684 Brassell, S.C., Eglinton, G., Marlowe, I.T., Pflaumann, U., Sarnthein, M., 1986.
685 Molecular stratigraphy: a new tool for climatic assessment, Nature, 320, 129–133,
686 https://doi.org/10.1038/320129a0.

687 Campos, E.J.D., Miller, J.L., Moiler, T.J., Peterson, R.G., 1995. Physical oceanography
688 of the Southwest Atlantic Ocean, Oceanography, 8, 87-91,
689 https://doi.org/10.5670/oceanog.1995.03.

690 Campos, E.J.D., Velhote, D., Silveira, I.C.A., 2000. Shelf break upwelling driven by
691 Brazil current cyclonic meanders, Geophys. Res. Lett., 27, 751-754,
692 https://doi.org/10.1029/1999GL010502.

693 Capron, E., Govin, A., Stone, E.J., Masson-Delmotte, V., Mulitza, S., Otto-Bliesner,
694 B., Rasmussen, T.L., Sime, L.C., Waelbroeck, C., Wolff, E.W., 2014. Temporal and
695 spatial structure of multi-millennial temperature changes at high latitudes during the Last

696 Interglacial, Quat. Sci. Rev., 103, 116-133, https://doi.org/10.1016/j.quascirev.2014.08.
697 018.

698 Ceccopieri, M., Carreira, R.S., Wagener, A.L.R., Hefter, J., Mollenhauer, G., 2018. On
699 the application of alkenone- and GDGT-based temperature proxies in the southeastern
700 Brazilian continental margin, Org. Geochem., 126, 43-56,
701 https://doi.org/10.1016/j.orggeochem.2018.10.009.

702 Chiessi, C.M., Ulrich, S., Mulitza, S., Pätzold, J., Wefer, G., 2007. Signature of the Brazil-
703 Malvinas Confluence (Argentine Basin) in the isotopic composition of planktonic
704 foraminifera from surface sediments. Mar. Micropaleontol., 64, 1–2, 52–66,
705 https://doi.org/10.1016/j.marmicro.2007.02.002.

706 Chiessi, C.M., Mulitza, S., Groeneveld, J., Silva, J.B., Campos, M.C., Gurgel, M.H.C.,
707 2014. Variability of the Brazil Current during the late Holocene. Palaeogeogr.
708 Palaeoclimatol. Palaeoecol., 415, 28–36, http://dx.doi.org/10.1016/j.palaeo.2013.12.005.

709 Chiessi, C.M., Mulitza, S., Mollenhauer, G., Silva, J.B., Groeneveld, J., Prange, M., 2015.
710 Thermal evolution of the western South Atlantic and the adjacent continent during
711 Termination 1, Clim. Past, 11, 915–929, https://doi.org/10.5194/cp-11-915-2015.

712 Conti, L.A., Furtado, V.V., 2006. Geomorfologia da Plataforma Continental do Estado
713 de São Paulo, Braz. J. Geol., 36 (2): 305-312.

714 Costa, K.B.; Cabarcos, E.; Santarosa, A.C.A.; Battaglin, B.B.F.; Toledo, F.A.L., 2016. A
715 multiproxy approach to the climate and marine productivity variations along MIS 5 in SE
716 Brazil: A comparison between major components of calcareous nannofossil assemblages
717 and geochemical records. Palaeogeography, Palaeoclimatology, Palaeoecology,
718 Amsterdam, v. 449, p. 275–288.

719 Cordeiro, L.G.M.S., Belem, A.L., Bouloubassi, I., Rangel, B., Sifeddine, A., Capilla, R.,
720 Albuquerque, A.L.S., 2014. Reconstruction of southwestern Atlantic sea surface
721 temperatures during the last Century: Cabo Frio continental shelf (Brazil), Palaeogeogr.
722 Palaeoclimatol. Palaeoecol., 415, 225–232, https://doi.org/10.1016/j.palaeo.2014.01.020.

723 Crampton-Flood, E.D., Peterse, F., Sinninghe Damsté, J.S., 2019. Production of branched
724 tetraethers in the marine realm: Svalbard fjord sediments revisited, Org. Geochem., 138,
725 103907, https://doi.org/10.1016/j.orggeochem.2019.103907.

726 Dauner, A.L.L., Mollenhauer, G., Bícego, M.C., de Souza, M.M., Nagai, R.H., Figueira,
727 R.C.L., Mahiques, M.M., de Melo e Souza, S.H., Martins, C.C., 2019. Multi-proxy
728 reconstruction of sea surface and subsurface temperatures in the western South Atlantic
729 over the last ~75 kyr. Quat. Sci. Rev., 215, 22–34.
730 https://doi.org/10.1016/j.quascirev.2019.04.020.

731 Evangelista, H., Gurgel, M., Sifeddine, A., Rigozo, N.R., Boussafir, M., 2014. South
732 Tropical Atlantic anti-phase response to Holocene Bond Events, Palaeogeogr.
733 Palaeoclimatol. Palaeoecol., 415, 21–27, https://doi.org/10.1016/j.palaeo.2014.07.019.

734 Figueiredo, T.S., Santos, T.P., Costa, K.B., Toledo, F., Albuquerque, A.L.S., Smoak,
735 J.M., Bergquist, B.A., Silva-Filho, E.V., 2020. Effect of deep Southwestern Subtropical
736 Atlantic Ocean circulation on the biogeochemistry of mercury during the last two
737 glacial/interglacial cycles, Quat. Sci. Rev., 239, 106368,
738 https://doi.org/10.1016/j.quascirev.2020.106368.

739 Gordon, A.L., 1986. Inter-ocean exchange of thermocline water, J. Geophys. Res.,
740 91(C4), 5037‑5046.

741 Govin, A., Chiessi, C.M. , Zabel, M., Sawakuchi, A.O., Heslop, D., Hörner, T., Zhang,
742 Y., Mulitza, S., 2014. Terrigenous input off northern South America driven by changes
743 in Amazonian climate and the North Brazil Current retroflection during the last 250 ka,
744 Clim. Past, 10, 2, 843–862, http://dx.doi.org/10.5194/cp-10-843-2014.

745 Govin, A., Capron, E., Tzedakis, P.C., Verheyden, S., Ghaleb, B., Hillaire-Marcel, C., St-
746 Onge, G., Stoner, J.S., Bassinot, F., Bazin, L., Blunier, T., Combourieu-Nebout, N., El
747 Ouahabi, A., Genty, D., Gersonde, R., Jimenez-Amat, P., Landais, A., Martrat, B.,
748 Masson-Delmotte, V., Parrenin, F., Seidenkrantz, M.S., Veres, D., Waelbroeck, C., Zahn,
749 R., 2015. Sequence of events from the onset to the demise of the Last Interglacial:
750 Evaluating strengths and limitations of chronologies used in climatic archives, Quat. Sci.
751 Rev., 129, 1–36, http://doi.org/10.1016/j.quascirev.2015.09.018.

752 Gray, W.R., Evans, D. 2019. Nonthermal influences on Mg/Ca in planktonic
753 foraminifera: a review of culture studies and application to the last glacial maximum.
754 Paleoceanography and Paleoclimatology, [s. l.], v. 34, p. 306-315,
755 https://doi.org/10.1029/2018PA003517.

756 Hansen, J., Sato, M., Hearty, P., Ruedy, R., Kelley, M., Masson-Delmotte, V., Russell,
757 G., Tselioudis, G., Cao, J., Rignot, E., Velicogna, I., Tormey, B., Donovan, B., Kandiano,
758 E., von Schuckmann, K., Kharecha, P., Legrande, A.N., Bauer, M., Lo, K.-W., 2016. Ice
759 melt, sea level rise and superstorms: evidence from paleoclimate data, climate modeling,
760 and modern observations that 2.0 °C global warming could be dangerous, Atmos. Chem.
761 Phys., 16, 3761–3812, https://doi.org/10.5194/acp-16-3761-2016.

762 Hoffman, J.S., Clark, P.U., Parnell, A.C., He, F. 2017. Regional and global sea-surface
763 temperatures during the last interglaciation. Science, [s. l.], v. 355, p. 276- 279.

764 Hopmans, E.C., Weijers, J.W.H., Schefuß, E., Herfort, L., Sinninghe Damsté, J.S.,
765 Schouten, S., 2004. A novel proxy for terrestrial organic matter in sediments based on
766 branched and isoprenoid tetraether lipids, Earth Planet. Sci. Lett., 224, 107–116,
767 https://doi.org/10.1016/j.epsl.2004.05.012.

768 Huguet, A., Fosse, C., Laggoun-Défarge, F., Delarue, F., Derenne, S., 2013. Effects of a
769 short-term experimental microclimate warming on the abundance and distribution of
770 branched GDGTs in a French peatland, Geochim. Cosmochim. Acta., 105, 294-315,
771 https://doi.org/10.1016/j.gca.2012.11.037.

772 Huguet, A., Coffinet, S., Roussel, A., Gayraud F., Anquetil, C., Bergonzini, L.,
773 Bonanomi, G., Williamson, D., Majule A., Derenne, S., 2019. Evaluation of 3-hydroxy
774 fatty acids as a pH and temperature proxy in soils from temperate and tropical altitudinal
775 gradients, Org. Geochem., 129, 1-13, https://doi.org/10.1016/j.orggeochem.2019.01.002.

776 Huguet, C., Martrat, B., Grimalt, J.O., Sinninghe Damsté, J.S., Schouten, S., 2011.
777 Coherent millennial-scale patterns in $U_{37}^{K'}$ and TEX_{86}^{H} temperature records during the
778 penultimate interglacial-to-glacial cycle in the western Mediterranean,
779 Paleoceanography, 26, PA2218, https://doi.org/10.1029/2010PA002048.

780 Kim, J.H., van der Meer, J., Schouten, S., Helmke, P.,Willmott, V., Sangiorgi, F., Koç,
781 N., Hopmans, E.C., Sinninghe Damste, J.S., 2010. New indices and calibrations derived
782 from the distribution of crenarchaeal isoprenoid tetraether lipids: implications for past sea
783 surface temperature reconstructions, Geochim. Cosmochim. Acta, 74, 4639-4654,
784 https://doi.org/10.1016/j.gca.2010.05.027.

785 Kim, J., Romero, O.E., Lohmann, G., Donner, B., Laepple, T., Haam, E., Sinninghe
786 Damsté, J.S., 2012. Pronounced subsurface cooling of North Atlantic waters off

787 Northwest Africa during Dansgaard-Oeschger interstadials. Earth Planet. Sci. Lett., 340,
788 95–102, doi: 10.1016/j.epsl.2012.05.018.

789 Leduc, G., Schneide, R., Kim, J.-H., Lohmann, G., 2010. Holocene and Eemian sea
790 surface temperature trends as revealed by alkenone and Mg/Ca paleothermometry, Quat.
791 Sci. Rev., 29, 989–1004, https://doi.org/10.1016/j.quascirev.2010.01.004.

792 Leininger, S., T. Urich, M. Schloter, L. Schwark, J. Qi, G. Nicol, J. Prosser, S. Schuster,
793 and C. Schleper, 2006. Archaea predominate among ammonia- oxidizing prokaryotes in
794 soils, Nature, 442, 806–809, doi:10.1038/nature04983.

795 Leonhardt, A., Toledo, F.A.L., Coimbra, J.C., 2013. The productivity history in the
796 southwestern atlantic as inferred from coccolithophore record for the last 130 kyr, Rev.
797 bras. paleontol. 16(3):361-374.

798 Lessa, D.V.O., Ramos, R.P., Barbosa, C.F., da Silva, A.R., Belem, A., Turcq, B.,
799 Albuquerque, A.L.S., 2014. Planktonic foraminifera in the sediment of a western
800 boundary upwelling system off Cabo Frio, Brazil, Mar. Micropaleontol., 106, 55–68,
801 https://doi.org/10.1016/j.marmicro.2013.12.003.

802 Lessa, D.V.O., Venancio, I.M., dos Santos, T.P., Belem, A.L., Turcq, B.J., Sifeddine, A.,
803 Albuquerque, A.L.S., 2016. Holocene oscillations of Southwest Atlantic shelf circulation
804 based on planktonic foraminifera from an upwelling system (off Cabo Frio, Southeastern
805 Brazil), The Holocene, 26, 1175–1187, https://doi.org/10.1177/0959683616638433.

806 Lessa, D.V.O., Santos, T.P., Venancio, I.M., Albuquerque, A.L.S., 2017. Offshore
807 expansion of the Brazilian coastal upwelling zones during Marine Isotope Stage 5, Glob.
808 Planet. Change, 158, 13–20, https://doi.org/10.1016/j.gloplacha.2017.09.006.

809 Lisiecki, L.E., Raymo, M.E., 2005. A Pliocene-Pleistocene stack of 57 globally
810 distributed benthic $\delta^{18}O$ records, Paleoceanography, 20, 1, 1–17,
811 https://doi.org/10.1029/2004PA001071.

812 Locarnini, R.A., Mishonov, A.V., Antonov, J.I., Boyer, T.P., Garcia, H.E., Baranova,
813 O.K., Zweng, M.M., Paver, C.R., Reagan, J.R., Johnson, D.R., Hamilton, M., Seidov, D.,
814 2013. World Ocean Atlas 2013, Volume 1: Temperature. NOAA Atlas NESDIS.

815 Lopes dos Santos, R.A., Spooner, M.I., Barrows, T.T., De Deckker, P., Sinninghe
816 Damsté, J.S., Schouten, S., 2013. Comparison of organic ($U^{K'}_{37}$, TEX^{H}_{86}, LDI) and faunal
817 proxies (foraminiferal assemblages) for reconstruction of late Quaternary sea surface
818 temperature variability from offshore southeastern Australia, Paleoceanography, 28, 377–
819 387, https://doi.org/10.1002/palo.20035.

820 Lourenço, R.A., Mahiques, M.M., Wainer, I.E.K.C., Rosell-Melé, A., Bícego, M.C.,
821 2016. Organic biomarker records spanning the last 34,800 years from the southeastern
822 Brazilian upper slope: links between sea surface temperature, displacement of the Brazil
823 Current, and marine productivity, Geo Mar. Lett., 36, 361-369,
824 https://doi.org/10.1007/s00367-016-0453-7.

825 Lutjeharms, J.R.E., 2006. The Agulhas Current, 329 pp., Springer, Berlin.

826 Luz, L.G., Santos, T.P., Eglinton, T.I., Montluçon, D., Ausin, B., Haghipour, N., Sousa,
827 S.M., Nagai, R.H., Carreira, R.S., 2020. Contrasting late-glacial paleoceanographic
828 evolution between the upper and lower continental slope of the western South Atlantic.
829 Climate of the Past, [s. l.], v. 16, p. 1245-1261.

830 Luz, L.G., 2019. Mudanças oceanográficas e climáticas nos últimos 50 mil anos no
831 sudoeste do Atlântico com base em registros de paleo-indicadores orgânicos e

832 inorgânicos na Margem Continental do Rio de Janeiro, Brasil. 188 f. Thesis (PhD in
833 Chemistry) - Pontifícia Universidade Católica do Rio de Janeiro, Rio de Janeiro, Brazil.

834 Mahiques, M.M., Silveira, I.C.A., Sousa, S.H.M., Fukumoto, M.M., 2005. Modern
835 sedimentation in the Cabo Frio upwelling system, An. Acad. Bras. Ciênc., 77, 535–548,
836 http://dx.doi.org/10.1590/S0001-37652005000300013.

837 Mahiques, M.M., Coaracy Wainer, I.K., Burone, L., Nagai, R., Sousa, S.H.M., Figueira,
838 R.C.L., Silveira, I.C.A., Bícego, M.C., Pavani, V.A.D., Hammer, Ø. 2009. A high-
839 resolution Holocene record on the Southern Brazilian shelf: Paleoenvironmental
840 implications. Quaternary International, [s. l.], v. 206, n. 1–2, p. 52-61.

841 Mann, M., Bradley, R., Hughes, M., 1998. Global-Scale Temperature Patterns and
842 Climate Forcing Over the Past Six Centuries, Nature, 392, 779-787,
843 https://doi.org/10.1038/33859.

844 Marino, G., Zahn, R., Ziegler, M., Purcell, C., Knorr, G., Hall, I. R., Ziveri, P., Elderfield,
845 H., 2013. Agulhas salt-leakage oscillations during abrupt climate changes of the Late
846 Pleistocene, Paleoceanography, 28, 599–606, doi:10.1002/palo.20038.

847 Mathias, G. L., Roud, S. C., Chiessi, C. M., Campos, M. C., Dias, B. B., Santos, T. P., et
848 al., 2021. A multiproxy approach to unravel late Pleistocene sediment flux and bottom
849 water conditions in the western South Atlantic Ocean. Paleoceanography and
850 Paleoclimatology, 36, e2020PA004058. https://doi.org/10.1029/2020PA004058.

851 Mollenhauer, G., Inthorn, M., Vogt, T., Zabel, M., Sinninghe Damsté, J.S., Eglinton, T.I.,
852 2007. Aging of marine organic matter during cross-shelf lateral transport in the Benguela
853 upwelling system revealed by compound-specific radiocarbon dating. Geochemistry,
854 Geophysics, Geosystems 8, Q09004, doi:10.1029/2007GC001603.

Müller, P.J., Kirst, G., Ruhland, G., von Storch, I., Rosell-Melé, A., 1998. Calibration of the alkenone paleotemperature index $U^{K'}_{37}$ based on core-tops from the eastern South Atlantic and the global ocean (60 °N – 60 °S), Geochim. Cosmochim. Acta, 62, 1757–1772, https://doi.org/10.1016/S0016-7037(98)00097-0.

Otto-Bliesner, B.L., Rosenbloom, N., Stone, E.J., Mckay, N.P., Lunt, D.J., Brady, E.C., Overpeck, J.T. 2013. How warm was the last interglacial? New model–data comparisons. Philosophical Transactions of the Royal Society A, London, v. 371, 20130097, doi: 10.1098/rsta.2013.0097.

Otto-Bliesner, B., Braconnot, P., Harrison, S.P., Lunt, D.J., Abe-Ouchi, A., Albani, S., Bartlein, P., Capron, E., Carlson, A., Dutton, A., Fischer, H., Goelzer, H., Govin, A., Haywood, A., Joos, F., LeGrande, A., Lipscomb, W., Lohmann, G., Mahowald, N., Nehrbass-Ahles, C., Peterschmitt, J.Y., Pausata, F.S.-R., Phipps, S., Renssen, H., 2016. Two Interglacials: Scientific Objectives and Experimental Designs for CMIP6 and PMIP4 Holocene and Last Interglacial Simulations, Clim. Past Discussions, 1-36, https://doi.org/10.5194/cp-2016-106.

Past Interglacials Working Group of PAGES, 2016. Interglacials of the last 800,000 years, Rev. Geophys., 54, 162–219, doi:10.1002/2015RG000482.

Pereira, L.S., Arz, H.W., Pätzold, J., Portilho-Ramos, R.C., 2018. Productivity evolution in the South Brazilian Bight during the last 40,000 years. Paleoceanogr. Paleocl., 33, https://doi.org/10.1029/2018PA003406.

Pessenda, L.C.R., Vidotto, E., De Oliveira, P.E., Buso, A.A., Cohen, M.C.L., Rossetti, D.F., Ricardi-Branco, F.B., Bendassolli, J.A., 2012. Late Quaternary vegetation and coastal environmental changes at Ilha do Cardoso mangrove, southeastern Brazil,

878 Palaeogeogr. Palaeoclimatol. Palaeoecol., 363-364, 57-68,
879 https://doi.org/10.1016/j.palaeo.2012.08.014.

880 Peterse, F., Kim, J.- H., Schouten, S., Kristensen, D.K., Koç, N., Sinninghe Damsté, J.
881 S., 2009. Constraints on the application of the MBT/CBT palaeothermometer at high
882 latitude environments (Svalbard, Norway), Org. Geochem., 40, 692–699,
883 doi:10.1016/j.orggeochem.2009.03.004.

884 Peterson, R.G., Stramma, L., 1991. Upper-level circulation in the South Atlantic Ocean,
885 Prog. Oceanogr., 26, 1–73, https://doi.org/10.1016/0079-6611(91)90006-8.

886 Piola, A.R., Matano, R.P., 2001. Brazil and Falklands (Malvinas) currents. In: Steele, J.
887 H., Thorpe, S. A., Turekian, K. K. (Eds.), Ocean Currents: A Derivative of the
888 Encyclopedia of Ocean Sciences, Elsevier Inc., 35-43, https://doi.org/10.1016/B978-0-
889 12-409548-9.10541-X.

890 Piola, A.R., Campos, E.J.D., Möller Jr., O.O., Charo, M., Martinez, C., 2000. Subtropical
891 Shelf Front off eastern South America, J. Geophys. Res. Ocean., 105, 6565-6578,
892 https://doi.org/10.1029/1999JC000300.

893 Pivel, M.A.G., Santarosa, A.C.A., Toledo, F.A.L., Costa, K.B., 2013. The Holocene onset
894 in the southwestern South Atlantic, Palaeogeogr. Palaeoclimatol. Palaeoecol., 374, 164–
895 172, https://doi.org/10.1016/j.palaeo.2013.01.014.

896 Portilho-Ramos, R.C., Ferreira, F., Calado, L., Frontalini, F., Toledo, M.B., 2015.
897 Variability of the upwelling system in the southeastern Brazilian margin for the last
898 110,000 years, Glob. Planet. Chang., 135, 179–189,
899 https://doi.org/10.1016/j.gloplacha.2015.11.003.

Poulton, A.J., Holligan, P.M., Charalampopoulou, A., Adey, T.R., 2017. Coccolithophore ecology in the tropical and subtropical Atlantic Ocean: New perspectives from the Atlantic meridional transect (AMT) programme, Prog. Oceanogr., 158, 150–170, https://doi.org/10.1016/j.pocean.2017.01.003.

Prahl, F.G.,Wakeham, S.G., 1987. Calibration of unsaturation patterns in long-chain ketone compositions for palaeotemperature assessment, Nature, 330, 367–369, https://doi.org/10.1038/330367a0.

Ribeiro, C.G., Lopes dos Santos, A., Marie, D., Pellizari, V.H., Brandini, F.P., Vaulot, D., 2016. Pico and nanoplankton abundance and carbon stocks along the Brazilian Bight, Peer, J 4, e2587, https://doi.org/10.7717/peerj.2587.

Richardson, P.L., 2007. Agulhas leakage into the Atlantic estimated with subsurface floats and surface drifters, Deep-Sea Res. Part I Oceanogr. Res. Pap., 54, 8, 1361–1389, https://doi.org/10.1016/j.dsr.2007.04.010.

Rodrigues, S.V., Marinho, M.M., Cubas Jonck, C.C., Gonçalves, E.S., Brant, V.F., Paranhos, R., Curbelo, M.P., Falcão, A.P., 2014. Phytoplankton community structures in shelf and oceanic waters off southeast Brazil (20 ° - 25 °S), as determined by pigment signatures, Deep. Res. Part I Oceanogr. Res. Pap., 88, 47-62, http://dx.doi.org/10.1016/j.dsr.2014.03.006.

Santos, T.P., Lessa, D.O., Venancio, I.M., Chiessi, C.M., Mulitza, S., Kuhnert, H., Govin, A., Machado, T., Costa, K.B., Toledo, F., Dias, B.B., Albuquerque, A.L.S., 2017a. Prolonged warming of the Brazil Current precedes deglaciations. Earth Planet. Sci. Lett., 463, 1–12, http://dx.doi.org/10.1016/j.epsl.2017.01.014.

922 Santos, T.P., Lessa, D.O., Venancio, I.M., Chiessi, C.M., Mulitza, S., Kuhnert, H.,
923 Albuquerque, A.L.S., 2017b. The impact of the AMOC resumption in the western South
924 Atlantic thermocline at the onset of the Last Interglacial. Geophys. Res. Lett., 44, 11, 547-
925 554, https://doi.org/10.1002/2017GL074457.

926 Santos, T.P., Ballalai, J.M., Franco, D.R., Oliveira, R.R., Lessa, D.O., Venancio, I.M.,
927 Chiessi, C.M.; Kuhnert, H., Johnstone, H., Albuquerque, A.L.S., 2020. Asymmetric
928 response of the subtropical western South Atlantic thermocline to the Dansgaard-
929 Oeschger events of Marine Isotope Stages 5 and 3. Quat. Sci. Rev., Oxford, v. 237, n.
930 106307.

931 Schlitzer, R., 2013. Ocean Data View, http://www.awi- bremerhaven.de/GEO/ODV.

932 Schmid, C., 2014. Mean vertical and horizontal structure of the subtropical circulation in
933 the South Atlantic from three-dimensional observed velocity fields, Deep. Res. Part I
934 Oceanogr. Res. Pap., 91, 50-71, https://doi.org/10.1016/j.dsr.2014.04.015.

935 Schouten, S., Hopmans, E.C., Schefuß, E., Sinninghe Damsté, J.S., 2002. Distributional
936 variations in marine crenarchaeol membrane lipids: a new tool for reconstructing ancient
937 sea water temperatures?, Earth Planet. Sci. Lett., 204, 265–274, doi: 10.1016 / S0012-
938 821X (02) 00979-2.

939 Schouten, S., Hopmans, E.C., Sinninghe Damsté, J.S., 2013. The organic geochemistry
940 of glycerol dialkyl glycerol tetraether lipids: A review. Org. Geochem. 54, 19-61.

941 Scussolini, P., Marino, G., Brummer, G.- J. A., Peeters, F. J. C., 2015. Saline Indian
942 Ocean waters invaded the South Atlantic thermocline during glacial termination II.
943 Geology, 43(2), 139–142. https://doi.org/10.1130/G36238.1.

944 Shah, S.R., Mollenhauer, G., Ohkouchi, N., Eglinton, T.I., Pearson, A., 2008. Origins of
945 archaeal tetraether lipids in sediments: Insights from radiocarbon analysis. Geochimica
946 et Cosmochimica Acta 72, 4577–4594.

947 Silveira, I.C.A., Schmidt, A.C.K., Campos, E.J.D., Godoi, S.S., Ikeda, Y., 2000. A
948 corrente do Brasil ao largo da costa leste brasileira, Rev. Bras. Oceanogr., 48, 171-183,
949 https://doi.org/10.1590/S1413-77392000000200008.

950 Sinninghe Damsté, J.S., Ossebaar, J., Abbas, B., Schouten, S., Verschuren, D., 2009.
951 Fluxes and distribution of tetraether lipids in an equatorial African lake: Constraints on
952 the application of the TEX86 palaeothermometer and BIT index in lacustrine settings,
953 Geochim. Cosmochim. Acta, 73, 4232–4249, doi:10.1016/j.gca.2009.04.022.

954 Sousa, S.H.M., De Godoi, S.S., Amaral, P.G.C., Vicente, T.M., Martins, M.V.A., Sorano,
955 M.R.G.S., Mahiques, M.M., 2014. Distribution of living planktonic foraminifera in
956 relation to oceanic processes on the southeastern continental Brazilian margin (23 °S –
957 25 °S and 40 °W – 44 °W). Continental Shelf Research, Oxford, v. 89, p. 76-87.

958 Stramma, L., England, M., 1999. On the water masses and mean circulation of the South
959 Atlantic Ocean, J. Geophys. Res. Ocean., 104, 20863–20883,
960 https://doi.org/10.1029/1999JC900139.

961 Ternois, Y., Sicre, M.A., Boireau, A., Conte, M.H., Eglinton, G., 1997. Evaluation of
962 long-chain alkenones as paleo-temperature indicators in the Mediterranean Sea. Deep-
963 Sea Res. Part I Oceanogr. Res. Pap., 44, 271–286, https://doi.org/10.1029/96PA00041.

964 Tierney, J.E., Russell, J.M., Eggermont, H., Hopmans, E.C., Verschuren, D., Sinninghe
965 Damsté, J.S., 2010. Environmental controls on branched tetraether lipid distributions in

966 tropical East African lake sediments, Geochim. Cosmochim. Acta, 74, 4902–4918,
967 doi:10.1016/j.gca.2010.06.002.

968 Tierney, J. E., Tingley, M., P., 2014. A Bayesian, spatially-varying calibration model for
969 the TEX_{86} proxy, Geochim. Cosmochim. Acta, 127, 83-186,
970 http://dx.doi.org/10.1016/j.gca.2013.11.026.

971 Tierney, J. E., Tingley, M., P., 2018. BAYSPLINE: A new calibration for the alkenone
972 paleothermometer, Paleoceanography and Paleoclimatology, 33, 281–301,
973 https://doi.org/10.1002/2017PA003201.

974 Turney, C.S.M., Jones, R.T., 2010. Does the Agulhas Current amplify global
975 temperatures during super-interglacials?, J. Quat. Sci., 25, 6, 839-843,
976 https://doi.org/10.1002/jqs.1423.

977 Venancio, I.M., Belem, A.L., Lessa D.O., Albuquerque, A.L.S., Mulitza, S., Schulz, M.,
978 Kucera, M., 2017. Calcification depths of planktonic foraminifera from the southwestern
979 Atlantic derived from oxygen isotope analyses of sediment trap material, Mar.
980 Micropaleontol., 136, 37–50, https://doi.org/10.1016/j.marmicro.2017.08.006.

981 Veres, D., Bazin, L., Landais, A., Toyé Mahamadou Kele, H., Lemieux- Dudon, B.,
982 Parrenin, F., Martinerie, P., Blayo, E., Blunier, T., Capron, E., Chappellaz, J., Rasmussen,
983 S. O., Severi, M., Svensson, A., Vinther, B., Wolff, E. W., 2013. The Antarctic ice core
984 chronology (AICC2012): an optimized multi- parameter and multi-site dating approach
985 for the last 120 thousand years. Climate of the Past, [s. l.], v. 9, p. 1733–1748,
986 doi:10.5194/cp-9-1733-2013.

Wainer, I., Prado, L.F., Khodri, M., Otto-Bliesner, B., 2014. Reconstruction of the South Atlantic Subtropical Dipole index for the past 12,000 years from surface temperature proxy, Sci. Rep., 4, 5291, https://doi.org/10.1038/srep05291.

Walsh, E.M., Ingalls, A.E., Keil, R.G., 2008. Sources and transport of terrestrial organic matter in Vancouver Island fjords and the Vancouver–Washington Margin: A multiproxy approach using d13Corg, lignin phenols, and the ether lipid BIT index, Limnol. Oceanogr., 53, 1054–1063, doi:10.4319/lo.2008.53.3.1054.

Weijers, J.W.H., Schouten, S., Spaargaren, O.C., Sinninghe Damsté, J.S., 2006. Occurrence and distribution of tetraether membrane lipids in soils: implications for the use of the TEX86 proxy and the BIT index, Org. Geochem., 37, 1680–1693, https://doi.org/10.1016/j.orggeochem.2006.07.018.

Wuchter, C., Schouten, S., Coolen, M.J.L., Sinninghe Damsté, J.S., 2004. Temperature-dependent variation in the distribution of tetraether membrane lipids of marine Crenarchaeota: Implications for TEX86 paleothermometry. Paleoceanography, Washington, v. 19, p. 1–10.

Zubkov, M.V., Sleigh, M.A., Burkill, P.H., Leakey, R.J.G., 2000. Picoplankton community structure on the Atlantic Meridional Transect: a comparison between seasons. Progress in Oceanography, Oxford, v. 45, p. 369-386.

SUPPLEMENTARY MATERIAL

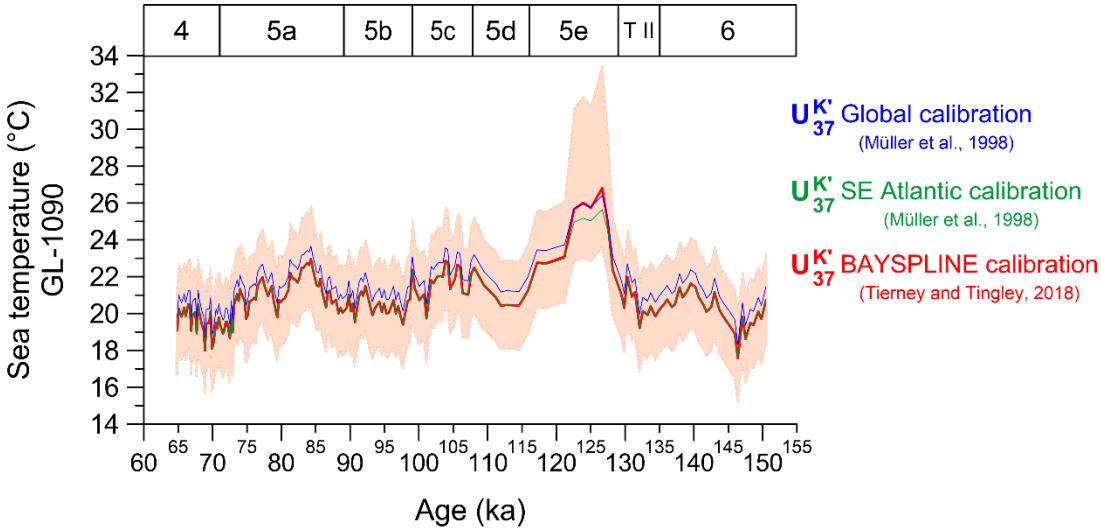

1007

1008 Supp. Fig. 1: Temp-$U^{K'}_{37}$ Global calibration - annual average (Müller et al., 1998) (blue),

1009 Temp-$U^{K'}_{37}$ SE Atlantic calibration - annual average (Müller et al., 1998) (green), and

1010 Temp-$U^{K'}_{37}$ BAYSPLINE calibration (Tierney and Tingley, 2018) (red) - red shading

1011 represents the 95% confidence interval. Marine isotope stages (MIS) are highlighted on the

1012 upper x-axis. (For interpretation of the references to color in this figure legend, the reader

1013 is referred to the web version of this article.)

1014

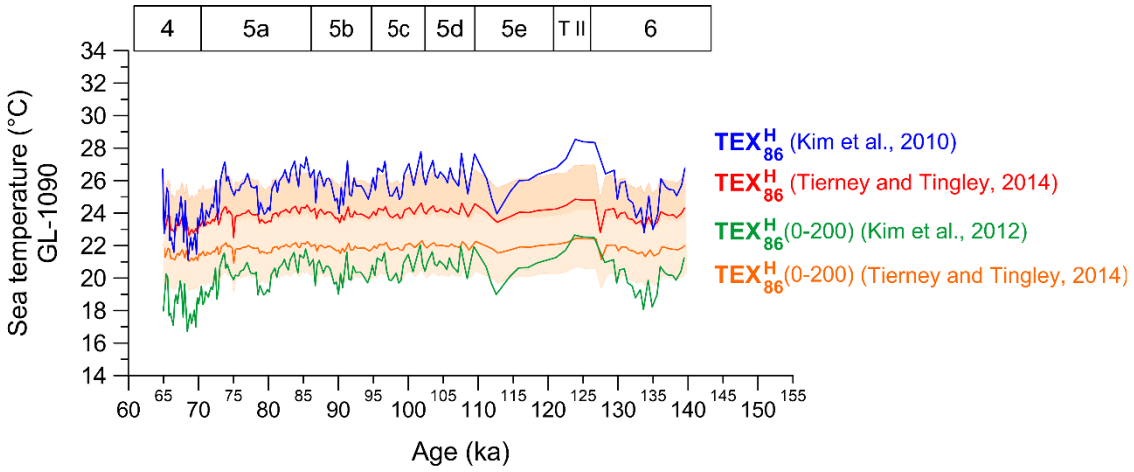

1015

1016 Supp. Fig. 2: Temp-TEX^{H}_{86} Global calibration - annual average (> 15 °C) (Kim et al.,

1017 2010) (blue), Temp-TEX^{H}_{86} (0-200) Global calibration - annual average (Kim et al., 2012)

1018 (green), Temp-TEX^{H}_{86} Bayesian calibration (Tierney and Tingler, 2014) (red) - red shading

represents the 95% confidence interval, and SubTemp-TEX_{86}^{H} Bayesian calibration (Tierney and Tingler, 2014) (orange) - orange shading represents the 95% confidence interval. Marine isotope stages (MIS) are highlighted on the upper x-axis. (For interpretation of the references to color in this figure legend, the reader is referred to the web version of this article.)

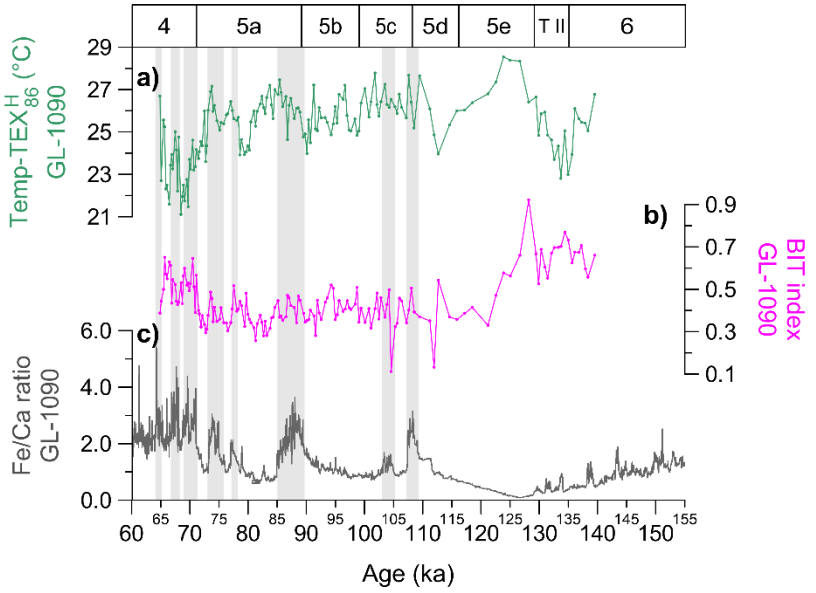

Supp. Fig. 3: Comparison between (a) Temp-TEX_{86}^{H} (green) (this study), (b) BIT index (pink) (this study) and (c) Fe/Ca ratio (gray) (Figueiredo et. al, 2020). Gray bars indicate peaks in Fe/Ca ratios. Marine isotope stages (MIS) are highlighted on the upper x-axis. (For interpretation of the references to color in this figure legend, the reader is referred to the web version of this article.)